



UNIVERSITY OF
CAMBRIDGE

Department of Engineering


Foundation Design for Floating Offshore Wind Turbines

Author Name: Charlie Spicer

Supervisor: Dr Christelle Abadie

Date: 27/05/2020

I hereby declare that, except where specifically indicated, the work submitted herein is my own original work.

Signed: 

Date: 27/05/2020

Technical Abstract

Foundation Design for Floating Offshore Wind Turbines

Author: Charlie Spicer Supervisor: Dr Christelle Abadie

The UK is committed to reducing its greenhouse gas emissions by 100% by 2050. One measure the government is taking to reach this target is the decarbonisation of the National Grid. The UK currently has 10GW of offshore wind capacity which produces around 25% of its renewable electricity and makes it the world leader in offshore wind installed capacity. With a flourishing industry, decreasing costs and a government target of 30GW of capacity by 2030, offshore wind is of significant importance to the UK's electricity supply and emissions reduction target.

As the offshore wind industry expands into deeper waters, it is expected that the superstructures and foundations of fixed-bottom offshore wind turbines will become prohibitively expensive, and therefore that floating offshore wind turbines will be used. There are only two operational commercial floating wind farms in the world – Hywind off the coast of Scotland and WindFloat Atlantic off the coast of Portugal.

Floating offshore wind turbines are therefore still in development, and one of the key technical barriers to their commercialisation is the design of their foundations. The associated design guidelines are limited by a lack of experience, and a dependence on existing guidelines for oil and gas offshore structures and fixed-bottom wind turbines.

This project focusses on the design of driven pile anchors in sand for use with Tension Leg Platforms (TLPs). TLPs are highly buoyant platforms, which are tethered to the seabed by high tension vertical tendons attached to anchors. External forces on the TLP such as the wind, waves and current create a purely tensile cyclic load on the anchor. This cyclic load will cause failure if not accounted for in the anchor's design.

To test the current design guidelines for TLP driven pile anchors, cyclic axial loading was applied to a test pile in sand to simulate the loading of the pile in the field.

First of all, the experimental procedure was developed so that pull-out tests on the test pile achieved a consistent ultimate capacity, T_{ULT} . It was found that driving the pile into position caused 'friction fatigue' in the sand and a significant variation in T_{ULT} achieved, compared to when the pile was wished-in-place.

Cyclic loading was applied to the test pile simulate different load cases and explore the different values of safety factors advised by the design guidelines. The subsequent

response of the pile was defined as unstable, meta-stable and stable. Safety factor were considered sufficient, if the pile behaved in a stable manner and showed an increase in ultimate capacity as a consequence of the cyclic loading.

The results were plotted on and showed good agreement with existing cyclic interaction diagrams for design.

It was found that the safety factor of 2.25 for extreme load cases recommended by the ABS design guidelines was insufficient, since the corresponding cyclic loading caused the test pile to behave in an unstable manner. On the other hand, the safety factor of 3 for normal load cases was potentially sufficient since the pile showed stable behaviour. However, unlike in other results from published literature, this stable test did not lead to an increase in the pile's ultimate capacity.

The results showed that decreasing the safety factor or increasing the severity of the load case applied to the test pile had a detrimental effect on the number of cycles that it could sustain. However, the main driver of the pile's response was the ratio of the cyclic amplitude of loading on the pile, to the pile's ultimate capacity (T_{CYC}/T_{ULT}). An increase in T_{CYC}/T_{ULT} caused cyclic degradation to occur faster and therefore the number of cycles to failure to decrease.

Two empirical logarithmic laws were derived to link the number of cycles sustained by a pile to the T_{CYC}/T_{ULT} ratio. These laws can be used by designers to ensure that a pile will be able to sustain the number of cycles expected during the TLP's lifetime.

Two empirical power laws were derived and recommended for N cycles of cyclic loading. The first can be used to predict the non-dimensional accumulated displacement ($\Delta\delta/\delta_s$) of a pile during unstable and meta-stable tests. This can be used in design codes to quickly calculate the displacement of the pile.

The second empirical law predicts the degradation in ultimate capacity of a pile, ΔT_{ULT} , as a consequence of cyclic loading. This empirical law can be used to predict the cyclic degradation experienced by a pile over its lifetime, so that a 'cumulative damage' approach to design can be used.

A corresponding interaction diagram was plotted, which can be used to predict the number of cycles to a pile's shaft failure for a given loading combination.

Table of Contents

Department of Engineering	1
List of major symbols.....	2
1. Introduction	3
2. Review of Literature.....	5
2.1. Current FOWT Concepts	5
2.2. Design Loads on Anchors.....	7
2.3. Design Guidelines	9
2.4. Cyclic Response	12
2.5. Project Objectives.....	15
3. Experimental Method.....	17
3.1. Test Rig.....	17
3.2. Sample Properties.....	19
3.3. Pile Geometry.....	22
4. Results and Discussions.....	28
4.1. Pull-out capacity	28
4.2. Cyclic response	28
5. Conclusions	42
6. Acknowledgements	44
7. References	45
8. Appendix A: Safety	48
9. Appendix B: COVID-19 Disruption	49

List of major symbols

δ	[L]	Pile head displacement
δ_N	[L]	Pile head displacement at cycle N
δ_0	[L]	Pile head displacements during monotonic loading
δ_s	[L]	Pile head displacement in static test due to T_{MAX}
$\Delta\delta$	[L]	Pile head displacement relative to 0 th cycle = $\delta_N - \delta_0$
D	[L]	Pile diameter
L	[L]	Pile length
N	[-]	Cycle number
N_i	[-]	Number of cycles to point of inflexion
$N_{0.1D}$	[-]	Number of cycles to displacement of 0.1D
N_a	[-]	Number of cycles to ‘point of acceleration’
N_f	[-]	Number of cycles to shaft failure
t	[L]	Pile thickness
T	[F]	Tension on anchor
T_{CYC}	[F]	Cyclic amplitude of tension on anchor
T_{MAX}	[F]	Maximum tension on anchor
T_{MEAN}	[F]	Mean tension on anchor
T_{MIN}	[F]	Minimum tension on anchor
T_{ULT}	[F]	Ultimate tensile capacity of anchor

Other symbols used throughout the report are explained in the text.

Test number notation

- 1) Pull-out tests are given the code:

PO-P-X

P is the pile used (B – bare, G – glued, S1 – sandpaper stage 1, S2 – sandpaper stage 2), and X is the test number (or Avg, where the average is taken)

- 2) Cyclic tests are given the code:

CYC-L-SF

L is the load case (N – normal, E – extreme), and SF is the safety factor at which the load case is applied. Where a cyclic test was not able to run for its full duration, a subsequent pull-out test was carried out, the code for which is:

PO-CYC-L-SF

1. Introduction

Climate change, caused by global warming due to the emission of greenhouse gases, is one of the greatest threats that society is currently facing.

In light of this, in its 2008 Climate Change Act, the UK Government set itself the target of being carbon neutral by 2050 (UK Government, 2019). One measure the government is taking to reduce its greenhouse gas emissions is to decarbonise the National Grid. The UK has made significant progress in this area, increasing the share of renewables in its electricity generation from 7% in 2010 to 33% in 2018. (BEIS, 2020)

The UK currently has 10GW of offshore wind capacity which produces around 25% of its renewable electricity. This makes the UK the world leader in offshore wind installed capacity, followed closely by Germany and China (Global Wind Energy Council, 2019). As well as this, the UK government’s Contracts for Difference (CfD) scheme has been highly successful at bringing down the cost of offshore wind electricity, such that by 2023 it is expected to be subsidy free and cheaper per MWh than existing gas plants. (Carbon Brief, 2019). With a flourishing industry, decreasing costs and a government target of 30GW of capacity by 2030, offshore wind is of significant importance to the UK’s electricity supply and emissions reduction target (BEIS, 2020).

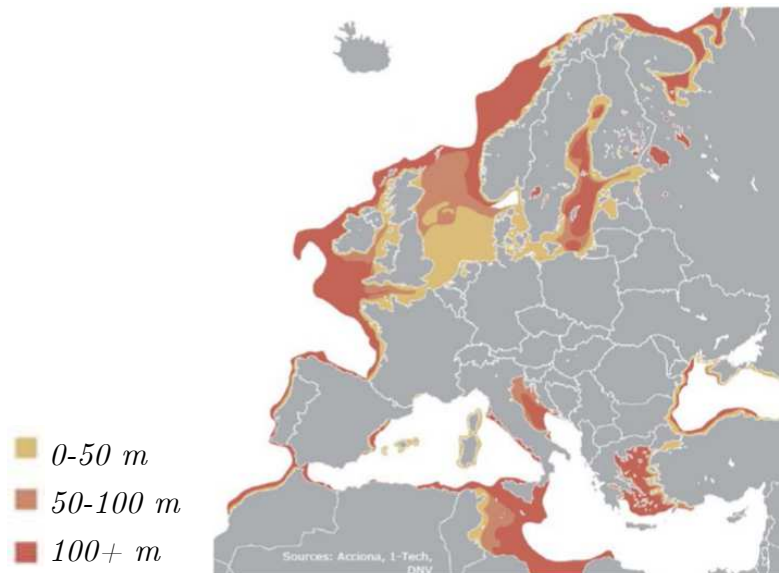


Figure 1.1: Sea depth around Europe (The Carbon Trust, 2015)

For the purposes of offshore wind farm construction, water depth can be classified into three classes: shallow waters (0-30m), transitional waters (30-50m) and deep waters (50-200m) (Oh, et al., 2018). Most of the world’s offshore wind farms are built in

shallow and transitional waters. However, most of the world's seas are not shallow (figure 1.1), and this necessitates the industry's expansion into deeper waters.

To access deeper waters, fixed-bottom turbines require heavier and more expensive super-structures and foundations. A solution is to use floating turbines. A floating offshore wind turbine (FOWT) is comprised of a floating platform supporting a turbine, tethered to the ground with tendons. It is estimated that FOWTs will be deployed in sea depths over 60m, in which their fixed-bottom counterparts are no longer economically viable. Over 8GW could be installed by 2050. (The Carbon Trust, 2015)



*Figure 1.2: (a) Hywind Scotland (equinor, n.d.),
(b) WindFloat Atlantic (Power Technology, 2020)*

There are currently only two commercially operating floating offshore wind farms in the world: Hywind Scotland completed in 2017 and located off the Scottish coast (equinor, n.d.) (figure 1.2(a)), and WindFloat Atlantic, due for completion in 2020 and located off the Portuguese coast (Power Technology, 2020) (figure 1.2(b)). However, there are over 30 concepts in development worldwide (The Carbon Trust, 2015).

The technology for FOWTs is hence currently under development, and there are several key technical barriers to its implementation and commercialisation. One of these is the design of the foundations which hold the FOWT's mooring lines in the ground. The Carbon Trust states that FOWT foundations and moorings could represent over 10% of their capital expenditure, and therefore identified improvements to the design of foundations as having great cost saving potential (The Carbon Trust, 2015).

The overall aim of this project is therefore to investigate a typical yet simple FOWT anchoring system, in order to inform on and improve its design.

2. Review of Literature

2.1. Current FOWT Concepts

2.1.1. Platform Types

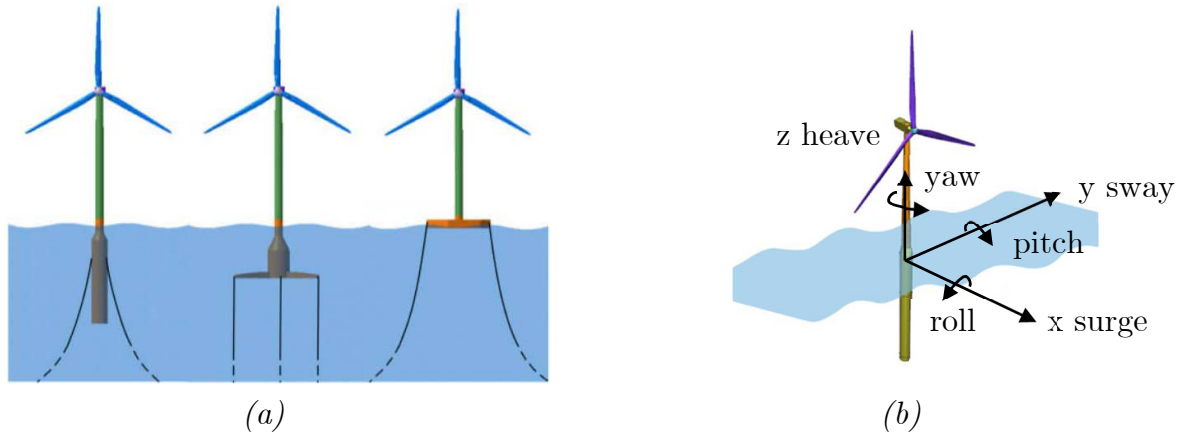


Figure 2.1: (a) Platforms types (Windpower Engineering and Development, 2018), L: Spar buoy, M: Tension Leg Platform (TLP), R: Semi-submersible platform, (b) 6 Degrees of freedom of FOWT (Yue, et al., 2020)

Current FOWT concepts can be split into 3 main categories based on the type of platform used (figure 2.1(a)).

A TLP's stability is provided by the vertical tendons which secure it to the seabed - of which there are typically three to eight. A TLP is similar to an upside-down pendulum oscillating about a vertical axis. Its platform is highly buoyant and its tendons under significant tension, and therefore any lateral force causing the TLP to deviate from this vertical position is met with a significant restoring moment.

Spar buoys on the other hand are stabilised by the large mass of their base, which ensures that the centre of mass of the platform is situated below their centre of buoyancy. Semi-submersible platforms are stabilised by the semi-submerged buoyant structures around their base.

Rather than the vertical taut-leg mooring system of TLPS, the most common mooring system for spar buoys and semi-submersible platforms is likely to be a catenary system (shown in figure 2.1(a)), though a semi-taut system could also be used. In a catenary system, each mooring line - of which there are typically three but up to nine - curves down from the platform, runs along the seabed, and is anchored at its end.

Due to its floating nature, a FOWT can move along 6 degrees of freedom, defined in figure 2.1(b). Motion in a particular degree of freedom can be described as compliant if displacement is measured in the order of metres, and restricted if in the order of centimetres. An example of restricted motion is the case of the elastic extension of TLP tendons, which allows only centimetres of heave motion.

Table 2.1: Typical FOWT motion, Restricted (R) or Compliant (C) (DNV-GL, 2018)

Platform	Surge	Sway	Heave	Roll	Pitch	Yaw
TLP	C	C	R	R	R	C
Spar buoy	C	C	C	C	C	C
Semi-sub	C	C	C	C	C	C

Each of the three platform types has its own advantages and disadvantages, and none has yet shown itself to be superior to the others. (The Carbon Trust, 2015)

Spar buoys were the first platform to be put into commercial use (Hywind, figure 1.2 (a)) and provide a simple design with few moving parts. However, they are restricted to deep waters over 100m, and – due to their deep base – cannot be constructed in a dry dock and require a heavy lift vessel for their assembly. (IRENA, 2016)

Semi-submersible platforms on the other hand can be easily constructed in a dry dock and towed to site through shallow waters. Of the three types they can also be installed in the shallowest waters (depths >40m). However, they are the heaviest of the three platforms due to their complicated steel structure, which also requires complicated welding and fabrication. (The Carbon Trust, 2015) (IRENA, 2016)

Tension leg platforms offer excellent stability (table 2.1) and the lowest structural mass. However, the loads on a TLPs tendon and anchor system are higher than for the other two platform types. (The Carbon Trust, 2015)

These high loads pose a particular problem to designers and make the average predicted capital expenditure on its anchors – £0.6m per turbine (The Carbon Trust, 2015) – greater than that of the other two platforms. However, costs can be significantly reduced by improvements in design. TLPs were therefore chosen as the focus of this project’s research.

2.1.2. Anchoring Systems

A range of anchoring systems originally developed for oil and gas operation could be used for FOWTs, namely drag-embedded anchors, gravity anchors, driven piles and suction piles. All are suitable for use with TLPs, other than drag embedded anchors, which are instead likely to be a popular choice for anchoring catenary mooring lines (The Carbon Trust, 2015).

The choice of TLP anchor will depend on the seabed conditions, the loads expected on the anchor at the site, and the specific design of TLP used. Of the three TLP anchoring systems, driven piles are the most versatile and are suitable for use in wide range of seabed conditions, including those with multiple layers of different soils. (The Carbon Trust, 2015)

Consequently, TLP driven pile anchors became the focus of this project's investigation. TLPs with driven pile anchors are also likely to be installed in the field in future, and therefore the project has potential real-world application.

2.2. Design Loads on Anchors

To date there is no standard for the maximum angle of inclination that a TLP's tendon can make to the vertical. Current research projects and prototypes have restricted the maximum angle in extreme environmental conditions to below 10° in some cases (Ng & Ran, 2016) (Pegalajar-Jurado, et al., 2016) and to below 5° in others (Suzuki, et al., 2011) (Zhao, et al., 2012).

Therefore, although the majority of the load on a TLP pile anchor is in the axial/vertical direction, lateral load components are present. It was decided that this project would simplify the loading on the anchor and only consider axial loading. Future research could investigate the effect of combined axial and lateral loading.

Each of a TLP's tendons is under significant axial tension. The tension varies dynamically as the FOWT is excited at different frequencies, but the pretension is sufficient to ensure that the tension never goes negative (DNV-GL, 2018). Tendons on the same TLP can have significantly different tensions. Figure 2.3(a) shows the external forces acting on a wind turbine, and figure 2.2(a) demonstrates the case in which the wind force on the turbine creates a moment on the platform. This leads to an increased tension in the upwind tendon, and a decreased tension in the downwind tendon.

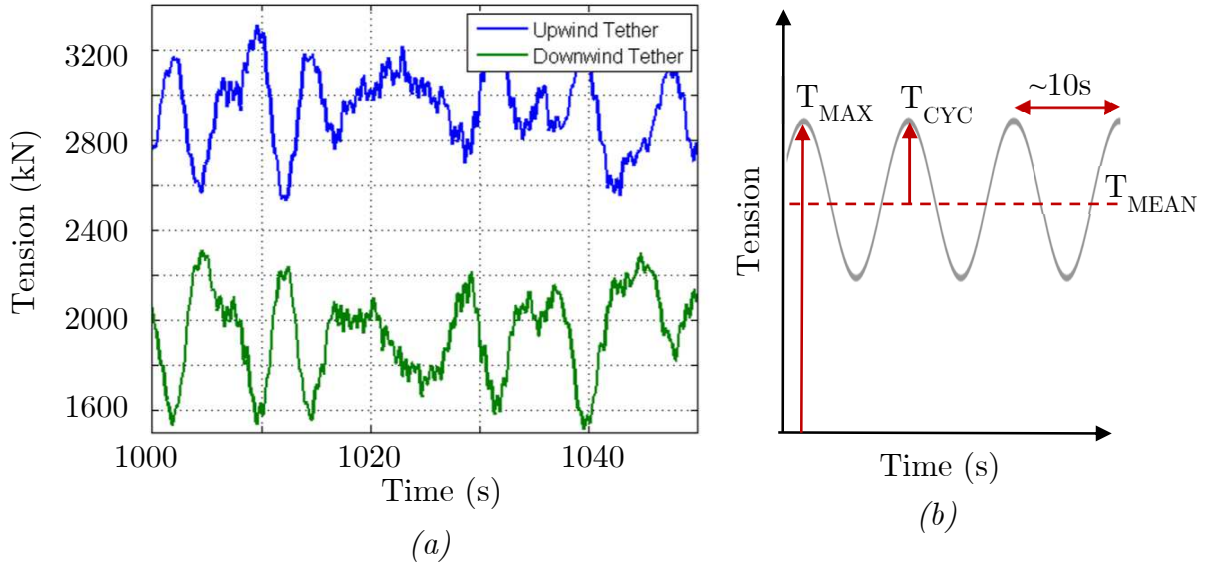


Figure 2.2: (a) Real tendon tension signal, operating conditions (Crozier, 2011)
 (b) Idealised tendon tension signal

The signal of a tendon's tension over time can be simplified into a mean component and a dynamic component (DNV-GL, 2018). The main constituents of the mean load are the tendon's pretension, the wind loading and the current loading. The majority of the dynamic component is created by the waves, turbine rotation and excitation of the platform's modes (Ng & Ran, 2016). As figure 2.3(b) shows, the wave loading typically dominates the dynamic loading on the tendon.

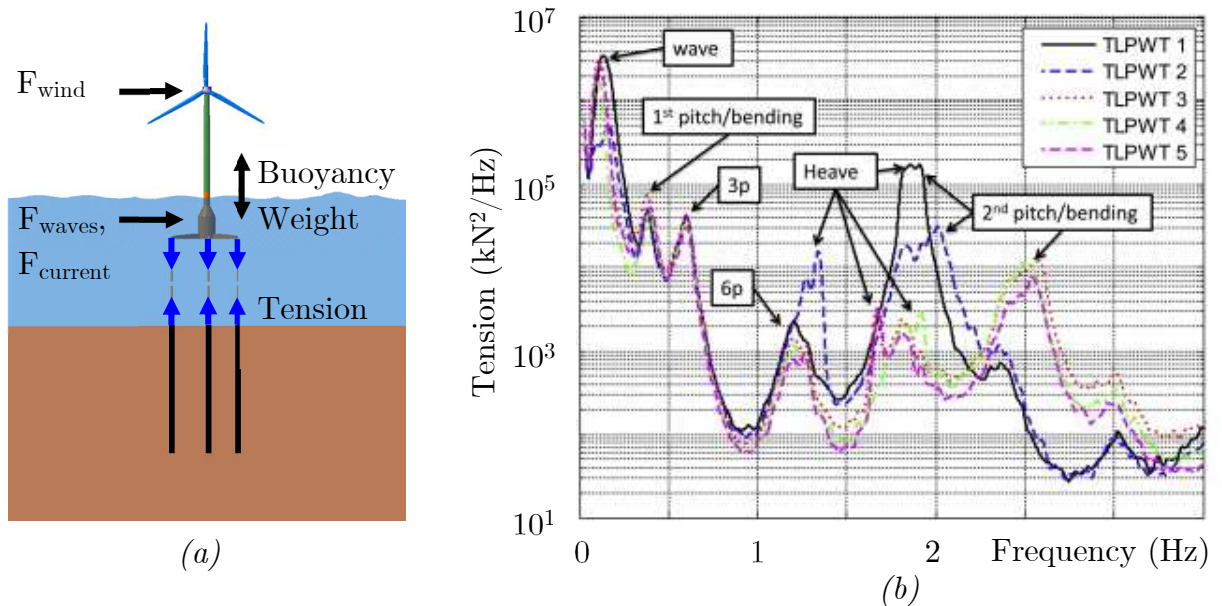


Figure 2.3: (a) External forces acting on a TLP,
 (b) Tendon tension vs frequency for 5 prototype TLPs,
 environmental condition: rated condition, significant wave height: 3.1m,
 peak wave period: 10.1s, mean wind speed: 11.4ms^{-1}
 Computationally modelled (Bachynski & Moan, 2012)

The frequency of offshore wave loading varies but the peak is generally around 0.1Hz. (Abadie, 2015). The tension in a TLP’s tendon can therefore be simplified into a sinusoidal cyclic load of frequency 0.1Hz, T_{CYC} , with mean, T_{MEAN} (figure 2.2(b)).

Very little data exists regarding the amplitude of cyclic loading, T_{CYC} , experienced by a tendon. The exact nature of the tension in each tendon, and therefore the tension on each anchor, depends on a range of variables including the specific design of TLP used and its specific location. Therefore, the values shown in table 2.2 are only intended to be used as an indication of the forces that could be experienced by a TLP’s tendon.

Table 2.2: Tendon tensions of concept TLPs

TLP design	Environmental conditions	T (kN)				Source
		MIN	MAX	CYC	CYC/MAX	
2.4MW TLP Japanese waters	Waves 12m Wind 50ms ⁻¹	527	4367	1920	0.44	(Suzuki, et al., 2011)
5MW TLP Gulf of Mexico	50-year hurricane	1620	11417	4899	0.43	(ABS, 2012)
5MW TLP	Waves 8m Wind 25ms ⁻¹	3080	7050	1985	0.28	(Matha, 2009)
10MW TLP	Waves 6m Wind 25ms ⁻¹	2500	3100	300	0.10	(Crozier, 2011)

2.3. Design Guidelines

Once the loads on a TLP’s driven pile anchor have been estimated, its required tensile strength (its ultimate capacity, T_{ULT}) can be estimated, and then it can be sized.

Many FOWT concepts are in development and prototyping stages, and therefore much of the data relating to their design is commercially sensitive and not publicly available. Industry design guidelines have made progress towards tackling this issue, with the classification societies DNV-GL leading the way in Europe and the American Bureau of Shipping (ABS) in the USA. (The Carbon Trust, 2015)

FOWTs are not a mature technology, and therefore much of their design is transferred from experience in the oil and gas industry and fixed-bottom wind turbine industry. In addition, the standard design approaches effectively ignore the effects of cyclic loading on the pile, which are instead accommodated by the use of safety factors, “expert engineering judgement and reasonably conservative assumptions” (Puech, 2013).

These could be limitations in the ABS and DNV-GL methods, and it was therefore decided that they would be the focus of the project. The methods are explained below.

2.3.1. DNV-GL design guidelines

The DNV-GL-ST-0119 standards contain the requirements and principles for the design of floating offshore wind turbines (DNV-GL, 2018), where the ultimate tensile capacity required of a driven pile anchor, T_{ULT} , is recommended as follows:

- 1) Firstly, the design tension in each tendon, T_d , is calculated using equation 1:

$$T_d = \gamma_{mean} T_{c,mean} + \gamma_{dyn} T_{c,dyn} \quad (1)$$

Table 2.3: Load factors

Limit state	Load factor	Consequence class	
		1	2
ULS	γ_{mean}	1.3	1.5
ULS	γ_{dyn}	1.75	2.2
ALS	γ_{mean}	1	1
ALS	γ_{dyn}	1.1	1.25

Where $T_{c,mean}$ and $T_{c,dyn}$ are the mean and dynamic components respectively of the 50-year value of the tendon tension. The load factors γ_{mean} and γ_{dyn} are given in table 2.3 for consequence classes 1 and 2 which describe FOWT systems with and without redundancy respectively. If a FOWT is designed with redundancy, a tendon or anchor can fail without the entire turbine failing.

- 2) A further safety factor, γ_m , is applied to determine T_{ULT} of the pile:

$$T_{ULT} = \gamma_m T_d \quad (2)$$

Where the safety factor $\gamma_m = 1.3$ at ULS and 1.0 at ALS.

- 3) “The effects of cyclic loading on the soil properties shall be considered“ (DNV-GL, 2018), and from these soil properties the size of the pile required to achieve T_{ULT} is calculated. There is no guidance on how this is achieved.

2.3.2. ABS design guidelines

In 2013, the ABS released a report titled “Offshore Anchor Data for Preliminary Design of Anchors of Floating Offshore Wind Turbines” (ABS, 2013), providing a design

method for TLP driven pile anchors. These are mostly transferred from the design methods for jacket-type fixed-bottom oil and gas platforms (API RP 2A (API, 2000)).

- 1) The maximum expected tensile load on the anchor T_{MAX} is estimated for each of four given load cases (those given in table 2.4). The return period of each load is not explicit, though 100 years is used for oil and gas applications (API, 2000).
- 2) An API recommended safety factor (table 2.4) is applied to the value of T_{MAX} for each load case. This results in four values of T_{ULT} , and whichever is greatest is used for the pile's design:

$$T_{ULT} = \max(T_{MAX} \times SF) \quad (3)$$

The B-factor in table 2.4 is an empirical value which aims to account for the uncertainty in pile design, load redistribution and several other aspects. The API suggest a minimum B-factor of 1.5 based on experience in the Gulf of Mexico. To the knowledge of the author, no other B-factors are publicly available for other scenarios or areas of the world.

Table 2.4: Safety factors for TLPs (API, 2010)

Load case	Safety Factor, SF	
Normal	2.0 x B	3.0
Extreme	1.5 x B	2.25
Damage (with reduced extreme environment)	1.5 x B	2.25
One tendon removed (with reduced extreme environment)	1.5 x B	2.25

- 3) The length L, diameter D, and thickness t of the piles are derived from the following equation, and the data in table 2.5.

$$L, D, t = c (T_{ULT})^d \quad (4)$$

Table 2.5: Constants required to derive L (m), D (m) and t (mm) (ABS, 2013)

Anchor Type	Soil	L (m)		D (m)		t (mm)	
		c	d	c	d	c	d
Driven Pile	Very Soft Clay	3.2744	0.3374	0.0655	0.3375	1.6390	0.3373
	Medium Clay	2.0402	0.3602	0.0407	0.3604	1.0197	0.3603
	Sand	2.1555	0.3333	0.0431	0.3334	1.0787	0.3332

The comparison in table 2.6 demonstrates that the ABS guidelines are more conservative than those of DNV-GL. Four different ratios of $T_{c,mean}$ to $T_{c,dyn}$ were input into each design method (in the ABS method it was assumed $T_{MAX}=T_{c,mean}+T_{c,dyn}$).

The ABS pile always had a higher T_{ULT} than the DNV-GL pile, despite the ABS T_{ULT} being set to its lowest value (assuming extreme loading, an SF of only 2.25) and the DNV-GL T_{ULT} being set to its highest value (assuming consequence class 2, no redundancy). It was therefore decided to investigate the ABS guidelines further.

Table 2.6: Comparison of DNV-GL and ABS T_{ULT} results for different loads

$T_{c,mean}$ (N)	$T_{c,dyn}$ (N)	DNV-GL T_{ULT} (N)	ABS T_{ULT} (N)
1	0.1	2.24	2.48
1	0.2	2.52	2.70
1	0.3	2.81	2.93
1	0.4	3.09	3.15

2.4. Cyclic Response

2.4.1. Interaction diagram

A further design method commonly used for the cyclic axial loading of piles is to use an interaction diagram. Interaction diagrams synthesise the effect of a mean, T_{MEAN} , and cyclic load, T_{CYC} , on the number of cycles to a pile's failure.

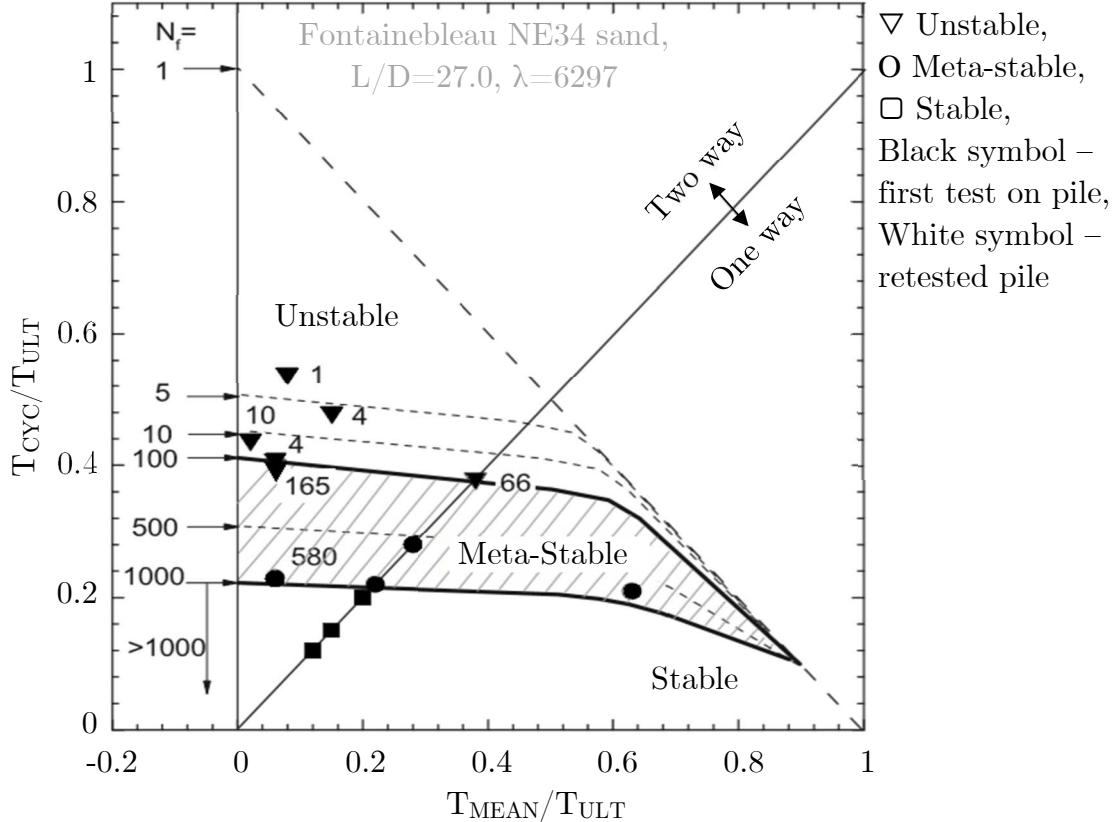


Figure 2.4: Interaction diagram (Tsuha, et al., 2012)

Note: symbols have been altered so that the interaction diagrams in this report match

Mainly due to the recent contributions of the SOLCYP project (SOLCYP, 2012), there are interaction diagrams for both sand and clay, for both tensile and compressive cyclic loading, derived from both field and lab tests (Puech, 2013). Two sets of data address the tensile cyclic loading of driven piles in sand. Figure 2.4 shows one from lab tests on an instrumented closed-ended pile (Tsuha, et al., 2012).

The second is from one-way cyclic loading tests on open-ended driven piles in Dunkirk sand (Jardine & Standing, 2012), and is therefore of particular relevance to the project. The two interaction diagrams lack data for the combinations of T_{CYC}/T_{ULT} and T_{MEAN}/T_{ULT} potentially experienced by a TLP's anchor. Therefore, this project's cyclic test results have the potential to provide a useful comparison and addition to Jardine and Standing's existing interaction diagram (analysis in section 4.2.4, figure 4.8).

The failure criteria in the two interaction diagrams are (Silva, et al., 2013):

- 1) Either: the pile head displacement, δ , exceeds $0.1D$
- 2) Or: the pile head displacement shows a rapid increase, indicating shaft failure

Each cyclic loading test was characterised as unstable if the number of cycles to failure N was < 100 , meta-stable if $100 < N < 1000$ or stable if $1000 < N$. Regions are plotted on the interaction diagrams in which it is theorised that the behaviour of the pile could generally be characterised as unstable, meta-stable and stable.

It was observed that unstable tests typically accumulated displacement rapidly and saw marked reductions in ultimate capacity, whereas during stable tests the pile's ultimate capacity increased, and displacements accumulated slowly until the pile effectively stabilised.

The term 'stable' is effectively arbitrary, as a TLP anchor will need to be able to sustain many more than 1000 cycles of cyclic loading during its lifetime. For example, in a single typical North Sea storm there at least 10,000 significant waves, and therefore at least 10,000 cycles (Jardine & Standing, 2000).

2.4.2. Degradation Law

Jardine and Standing also proposed a simple method for predicting the reduction of a pile's shaft resistance, and therefore the reduction in its ultimate capacity ΔT_{ULT} , as a result of cyclic loading (Andersen, et al., 2013). The empirical degradation law in equation 5 has been adapted using this project's symbols (Jardine & Standing, 2012).

$$\frac{\Delta T_{ULT}}{T_{ULT}} = A \left(B + \frac{T_{CYC}}{T_{ULT}} \right) N^C \quad (5)$$

A, B and C are constants (-0.126, -0.1 and 0.45 respectively), set to fit their results.

According to the law, the effect of T_{MEAN} on the degradation of T_{ULT} is negligible (and it is therefore absent from equation 5). This is the case as long as equation 6 is satisfied.

$$\frac{\tau_{vh}}{\sigma'_v} < \tan \delta \quad (\text{Note: equivalent to } K_0 < 1) \quad (6)$$

Where τ_{vh} is the peak horizontal shear stress, σ'_v is the effective stress, δ is the soil pile friction angle and K_0 is the coefficient of earth pressure at rest (=0.45 in this project).

During cyclic loading, a pile's strength typically gradually degrades until it can no longer sustain the applied load. Therefore, in a load-controlled experiment, a pile's ultimate capacity will drop until it reaches T_{MAX} . At this point shaft failure occurs, and the pile head displaces rapidly. This is shown in figure 2.5(a).

Therefore, at shaft failure, $\Delta T_{ULT} = T_{MAX} - T_{ULT}$. Equations 7 and 8 demonstrate how – by taking $T_{MAX} = T_{CYC} + T_{MEAN}$ – equation 5 can be rearranged to plot another interaction diagram (figure 2.5(b)). This interaction can be used to predict the number of cycles to shaft failure, N_f , for different combinations of loading.

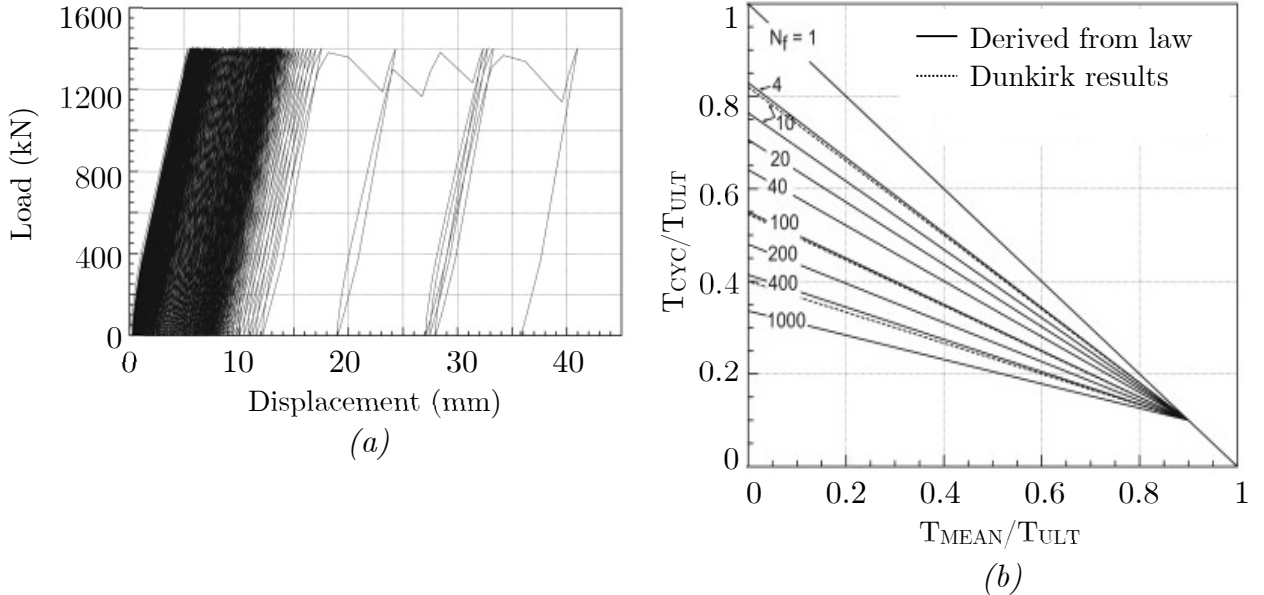


Figure 2.5: (a) Load-displacement graph for metastable cyclic loading, 208 cycles (Jardine & Standing, 2012),

(b) Shaft failure interaction diagram (Jardine & Standing, 2012)

Note: the interaction diagrams of figure 2.4 and figure 2.5(b) differ, since in figure 2.5(b) failure is defined as shaft failure only, not displacement by 0.1D.

$$\frac{T_{CYC} + T_{MEAN} - T_{ULT}}{T_{ULT}} = A \left(B + \frac{T_{CYC}}{T_{ULT}} \right) N_f^c \quad (7)$$

$$\frac{T_{CYC}}{T_{ULT}} = \frac{\frac{T_{MEAN}}{T_{ULT}} - 1 - A B N_f^c}{A N_f^c - 1} \quad (8)$$

2.4.3. Displacement Law

It is useful for designers to be able to predict the displacement of a pile after N cycles of loading. This is because a pile can be prevented from displacing too far (e.g. a design limit such as $0.1D$), or from displacing relative to the other piles, and therefore causing unbalanced tensions in the TLP's tendons.

An empirical displacement law exists for the lateral cyclic loading of piles, in which the angle of rotation of a pile after its initial monotonic rotation, $\Delta\theta$, increases with N according to equation 9. (Leblanc, et al., 2010a)

$$\frac{\Delta\theta}{\theta_s} = T_0 N^{0.31} \quad (9)$$

Where θ_s is the rotation of the pile “that would occur in a static test when the load is equivalent to the maximum cyclic load” (Leblanc, et al., 2010a), and T_0 is a function of the relative density of the sand I_D , and the force ratios ζ_b and ζ_c (T_{MAX}/T_{ULT} and T_{MIN}/T_{MAX} respectively).

2.5. Project Objectives

The ABS design guidelines are based on designs for the oil and gas industry, have safety factors applying to the Gulf of Mexico only, and do not account for cyclic loading (other than applying large safety factors). These could be serious limitations in the design of TLP driven pile anchors.

The safety factors in the design method will be investigated to determine whether, despite these limitations, they might still enable a safe design. A suitable safety factor in the field will ensure that each anchor withstands a lifetime of loading (20+ years) (The Carbon Trust, 2015), but is not overly-conservative, and therefore leads to unnecessary material usage and cost.

In the following cyclic loading tests, a safety factor will be considered safe if the pile behaves in a stable manner and its ultimate capacity does not degrade.

There are 5 main milestones in the investigation.

- 1) Design a pile based on the ABS guidelines. Determine the ultimate capacity, T_{ULT} , of the pile in sand.
- 2) Carry out one-way cyclic loading tests on the pile at different amplitudes, T_{CYC} , and maximum values, T_{MAX} (details can be found in table 2.7). The aim is to simulate different load cases (normal and extreme) at different safety factors.

The two load cases, “normal” and “extreme”, have amplitudes T_{CYC}/T_{MAX} of 0.2 and 0.4 respectively. There is no set T_{CYC} which defines normal or extreme loading, instead these are designed to be estimates of the loads that might be experienced by a TLP’s anchor during these load cases (section 2.2).

The design method uses a safety factor of 2.25 for extreme loading and 3.0 for normal loading. These are tested, as well as a safety factor of 1.5 (which has been included so that a range of behaviour from stable to unstable is observed).

Table 2.7: Test programme

Test	Load case	T_{CYC}/T_{MAX}	Safety factor	T_{ULT}/T_{MAX}
Pull-out	-	-	-	1
CYC-E-1.5	Extreme	0.4	1.5	1.5
CYC-E-2.25	Extreme	0.4	2.25	2.25
CYC-N-1.5	Normal	0.2	1.5	1.5
CYC-N-2.25	Normal	0.2	2.25	2.25
CYC-N-3	Normal	0.2	3	3

- 3) Each test is classified as stable, meta-stable or unstable, and the results are plotted on Jardine and Standing’s interaction diagram for comparison, and to provide additional data specific to TLPs.
- 4) An empirical displacement law like that of equation 9 is found to relate the number of cycles applied to a pile N to its displacement δ .
- 5) Equation 5 is fit to the results, so that the degradation of a pile’s ultimate capacity can be predicted. An interaction diagram like that of figure 2.5(b) is plotted, which can be used to predict the number of cycles until a pile experiences shaft failure.

3. Experimental Method

3.1. Test Rig

The Schofield Centre's cyclic test rig was used for the tests (figure 3.1). It was originally designed by Rovere in 2004 for the axial loading of suction piles in sand (Rovere, 2004), and has subsequently been modified and used to investigate the lateral loading of piles in sand by Leblanc and Abadie (Leblanc, et al., 2010a; Abadie, 2015).



(a) Rig and Data Acquisition Computer



(b) LVDT, Load cell and Pile set-up



(c) Mass 2



(d) Lever arm, Motor and Mass 1

Figure 3.1: Experimental rig components

Figure 3.2 shows the test rig in its current set up, having been modified for the purposes of this project to convert it from laterally loading short rigid piles, to axially loading long slender piles. Originally, the sand and pile were installed in the clear box. Cable 1 was attached to the pile head, and Cable 2 held the counterweight, Mass 2.

A pile with a length in the order of 1m was required, and therefore the depth of clear box (400mm) was not sufficient. A new container was found with depth 1000mm. The container was placed outside the rig, and the roles of Cable 1 and 2 were switched.

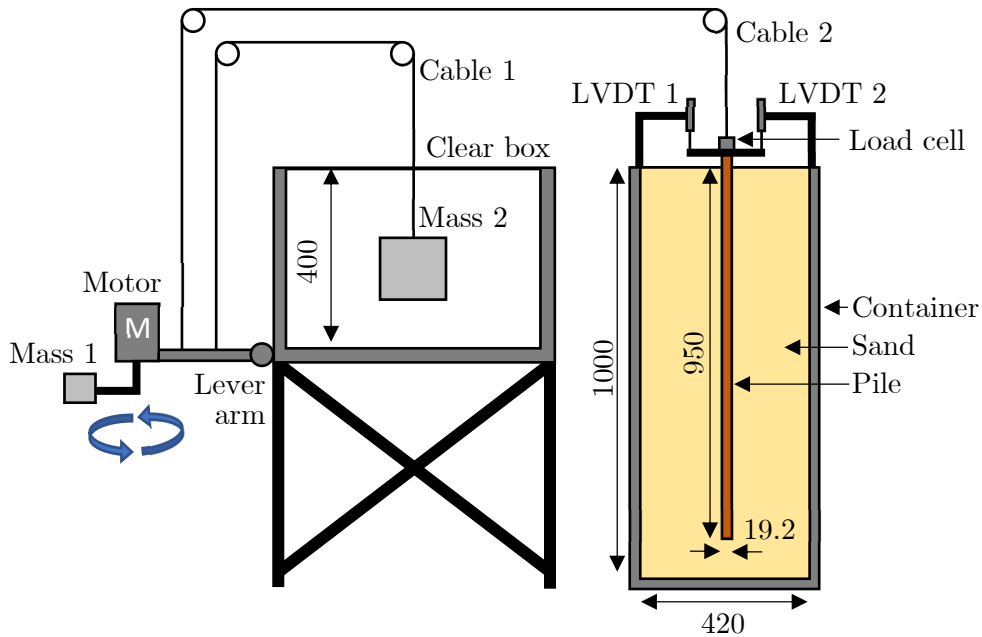


Figure 3.2: Test rig schematic diagram (dimensions in mm)

In its current set up the rig is load controlled. Cyclic loading is applied by a motor driving a rotating mass, Mass 1, on the end of a lever arm. This creates a sinusoidally fluctuating moment about the lever arm pivot, and therefore a sinusoidally fluctuating tension on the pile via Cable 2. Mass 2 acts as a counterweight, and by adjusting its value and that of Mass 1, the mean and cyclic amplitude of the force can be varied.

The motor runs at a frequency of 0.106Hz, applying a load of similar frequency to wave loading. It is therefore capable of applying 10,000 cycles in around 26 hours.

2.3.1. Transducers

The following transducers were used to record the force on the pile and its displacement.

- **Load cell:** the sinusoidally varying tension on the pile head is measured by the load cell. The loadcell measured up to 200N with a voltage range of $\pm 5V$. The resolution of $20NV^{-1}$ meant highly precise readings could be taken
- **LVDT 1 and 2:** the pile's displacement was measured by two LVDTs, and an average of their readings was taken to ensure the results were not affected by any pile head tilting. Both LVDTs were Solartron DFG 5.0s, with a voltage range of $\pm 5V$ and working range of $\pm 5mm$ (though during tests $\pm 7.5mm$ was achieved), enabling measurement of small displacements with high resolution
- **Data Acquisition:** The loadcell and LVDT signals were logged by DASyLab software on a Schofield Centre Remote Data Acquisition Computer.

3.2. Sample Properties

3.2.1. Container dimensions and boundary conditions

A new sand container capable of holding a pile length in the order of 1m was set up for this project. The container needed to be large enough to satisfy the boundary condition of the experiment, but not so large that it became impractical to fill with sand. A cylindrical steel piston of height 1000mm and diameter 420mm (figure 3.3) was available and used as it satisfied the boundary conditions detailed below.



Figure 3.3: Sand container, (a) interior with depth markings, (b) filled with sand

The influence zone around the axially loaded pile needed to be smaller than the container, such that the sand interacted with static sand, not the container's edges.

1) Container height

For a pile under vertical compressive loading, the influence zone extends below the pile tip $3.5D$ to $5.5D$ for clean sands (Yang, 2006).

No such empirical influence zone exists for a pile in tension. However, there is no end bearing on a pile in tension, and therefore the sand below the pile is unlikely to play a significant role in its behaviour. Therefore, for pragmatic reasons during sample preparation, a clearance of less than $3.5D$ was allowed. The final pile had a length L of 950mm and diameter D of 19.2mm. This left a clearance of 50mm, $2.6D$.

2) Container Diameter

Little information is available in published literature on the optimal clearance for a pile in sand being tested at 1g.

When testing the effect of different $D_{\text{container}}/D_{\text{cone}}$ ratios on CPT cone resistance, Bolton found that as long as $D_{\text{container}}/D_{\text{cone}} > 44$, the cone resistance was unaffected (Bolton, et al., 1998). Taking D_{cone} to be synonymous with D , this would suggest $D_{\text{container}}/D > 44$. However, this boundary condition was impractical, since – for a 19.2mm diameter pile – it would require an 845mm diameter container.

More practical guidance came from Jardine and Standing’s tests in Dunkirk sand in which a spacing of $15D$ was used (Puech, 2013), and the cyclic testing of 1m long, 0.5 m wide piles in which the container’s diameter was $5D$ (Thomassen, et al., 2017).

The final pile diameter was 19.2mm, meaning the container diameter was $22D$ (table 3.1, figure 3.4). This was deemed suitably large to satisfy the boundary conditions, and for any effect on the results to be negligible.

Table 3.1: Final Container properties

Property	Value
Diameter	420mm
Depth	1000mm
Diameter relative to pile	$22D$
Pile clearance from bottom	$2.6D$ (50mm)

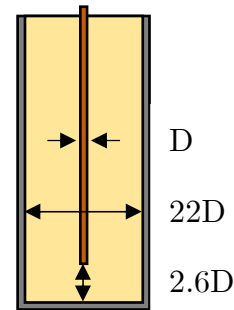


Figure 3.4: Final pile to container ratios

3.2.2. Sample properties

The experimental tests were conducted in dry Hostun Sand HN31, poured manually in order to achieve a low relative density, and therefore limit the effects of dilation.

In the field the sands are generally saturated with water. However, at the low frequency at which the tests run (0.106Hz), the loading can be assumed to be quasi-static, and so inertia effects and the build-up of excess pore pressure are unlikely to occur (Achmus, et al., 2005). Therefore, the sand behaves in a drained state, and for the purposes of the project, the tests can be carried out using dry sand.

A comparison between Hostun Sand and Dunkirk Sand is made in table 3.2. Dunkirk Sand is representative of sands found in the Southern North Sea (Jardine & Standing, 2000) and has been used by several research groups exploring the axial loading of piles including Imperial College London, and the GOPAL project (Rimoy, 2013). In particular it is the sand used by Jardine and Standing in the tests which produced their empirical degradation law (section 2.4.2, equation 5) and interaction diagram (section 4.2.5, figure 4.8), which are both used in this project.

Table 3.2: Hostun and Dunkirk Sand Properties

Property	Symbol	Unit	Hostun Sand	Dunkirk Sand ¹
Minimum void ratio	e_{\min}	-	0.555	0.57
Maximum void ratio	e_{\max}	-	1.01	0.91
Specific gravity	G_s	-	2.65	2.65
Critical angle of friction	ϕ_{crit}	degrees	33	32.1
Mean particle size	d_{50}	mm	0.424	0.269
Uniformity coefficient	C_u	-	1.67	1.56

¹ (Liu, et al., 2017)

3.2.3. Sand pouring

The tests are carried out at 1g, a much lower effective stress than in the field. This means the experimental sand will be able to dilate more than the sand in the field. The more sand dilates, the greater its peak friction angle. This might lead to an overprediction of the ultimate capacity of the pile, T_{ULT} . By pouring samples loose (a relative density of 8% was achieved in the tests) this effect is reduced, and represents a pile installed in a much denser sand profile at full-scale.

Many different methods were considered as to how the sand could be poured. Ideally, the Schofield Centre's automatic sand pourer would have been used. However, the container was too tall to fit underneath its nozzle.

In the end, the sand was poured manually. A small scoop was used to pour the sand slowly from a height of about 1cm onto the sand below. The sand was weighed before being put in the container, so that the unit weight and relative density of each test could be calculated. The advantage of manual pouring was that the process was very easy to control. It was also one of the only methods in which such a low relative density could be achieved, since the sand was being poured from such a low height.

3.2.4. Sample scaling

The empirical scaling law in equation 10 can be used to estimate the relative density of sand in the field that an experimental set up represents (Bolton, 1986).

$$I_R = I_D(10 - \ln p') - 1 \quad (10)$$

Where I_R is the relative dilatancy, I_D is the relative density and p' is the effective mean confining stress on the pile in kPa, at the pile's half-length. I_D in the field would be found by setting I_R at the half-length of a typical TLP pile in Dunkirk Sand, to match

I_R at the half-length of the test pile in Hostun Sand. However, an equivalent relative density could not be found.

Tests carried out at 1g are at very low confining stress, and therefore the relative density of the sand Hostun Sand needs to be very low to limit the effects of dilation. Each test was poured consistently to a relative density of 8%. However, this leads to a negative relative dilatancy I_R , which cannot be used with equation 10 to predict the relative density of sand in the field. No robust scaling law exists in literature for sands at such low confining stresses and relative densities.

3.3. Pile Geometry

3.3.1. Test pile design

A test pile needed to be designed to satisfy 3 constraints.

- 1) $L/D = 50$ and $D/t = 40$ as per the ABS design guidelines

Due to the standard sizes in which pipes are manufactured, it was not possible to find a thin enough tube to achieve $D/t = 40$. This is shown in table 3.3.

The pile's thickness, t , has a large effect on the strength and stiffness of the pile itself, but little effect on the pile's ultimate capacity in sand. This is because the test pile is under constant tension, so the majority of its capacity comes from the skin friction on its sides, not end-bearing. The D/t constraint was therefore relaxed.

- 2) A stiffness ratio, λ , equal to that in the field.

$$\lambda = \frac{E_p}{G_0} \quad (11)$$

Where the pile stiffness, E_p :

$$E_p = \frac{E_m \pi D t}{\pi D^2 / 4} \quad (12)$$

It was not possible to directly measure the initial shear modulus, G_0 , in the lab. Different methods can be used estimate to G_0 , and the following was used assuming a relative density of 8% and therefore a voids ratio, e , of 0.97 (p' is in MPa, and is calculated at the half length of the pile). (Haigh, 2020; Hardin & Drnevich, 1972)

$$G_0 = 100 \frac{(3 - e)^2}{(1 + e)} (p')^{0.5} \quad (13)$$

Table 3.3 shows the test pile options available, and the corresponding stiffness ratios.

Table 3.3: Test pile options

Property	Option 1	Option 2	Option 3	Field	Final pile
Material	Steel	Brass	Acrylic	Steel	Acrylic + Sandpaper
L x D x t	952.5mm x 3/4inch (19.05mm) x 16SWG (1.626mm)	952.5mm x 3/4inch (19.05mm) x 1/16inch (1.587mm)	900mm x 18mm x 3mm	65m x 1300mm x 32.5mm (ABS guidelines)	950mm x 19.2mm x 3.6mm
L/D	50	50	50	50	50
D/t	11.7	12	6	40	5.3
E _m GPa	210	110 ¹	3.2 ¹	210	3.2 ³
E _p GPa	71.8	36.7	2.1	21	2.4
G ₀ MPa	13.5	13.5	13.1	125.0 ²	13.5
λ	5320	2720	160	168	178

1 (The Engineering Toolbox, n.d.) 2 (Jardine & Standing, 2000) 3 A satisfactory value for the young's modulus of sand paper could not be found or calculated. EM for acrylic (3.2GPa) was used, as it was assumed to be of the correct order of magnitude.

An acrylic pile was chosen, due to its similar stiffness ratio λ to that of the field.

3) As high an ultimate capacity, T_{ULT} , as possible

The loads that can be applied using the test rig are finite, and therefore the pile needed an ultimate capacity of at least 50N for cyclic loading to be feasible. Also, the greater the ultimate capacity of the pile the greater the loads that can be applied, and therefore the better the signal to noise ratio of the experimental measurements.

$$T_{ULT} = P_{outside} + W_{pile} + W_{plug} \quad (14)$$

$$P_{outside} = \iint \sigma'_h \tan \delta dA = \pi D \int_0^L \sigma'_v K \tan \delta dz = \pi D \frac{\gamma' L^2 K \tan \delta}{2} \quad (15)$$

A pile's ultimate tensile capacity in sand is calculated as the sum of the skin friction, $P_{outside}$, the pile's weight, W_{pile} , and – if the pile plugs with sand during driving – the weight of the plug, W_{plug} . (Houlsby, 2009)

K is an empirical factor taken as 0.8 for an open-ended pile and δ is the soil-pile friction angle, which has been taken as 15° for very loose sands (API, 2000). This value of δ is for steel-sand interaction, and it was originally assumed that the acrylic-sand interaction would not be too dissimilar. The effective unit weight γ' is the same as the dry unit weight γ_d , since the Hostun is dry.

$$W_{plug} = \frac{\gamma' L \pi (D - 2t)^2}{4} \quad (16)$$

If the pile is driven, it is predicted that the pile will plug with sand if:

$$\frac{L}{D} > \frac{N_c}{4\alpha} \quad (17)$$

Where α is an empirical factor typically in the range 0.3 to 0.8, and N_c is an empirical factor conventionally taken as 9 (API, 2000; Houlsby, 2009). For tests in which the pile was installed by driving, it was assumed the pile would plug, since $L/D = 50$ and the maximum $N_c/4\alpha = 7.5$. In later tests the pile was wished-in-place and plugging did not occur (section 3.3.3).

These values – for the initial pile iteration (the bare pile) – are summarised in table 3.4. The ultimate capacity of 69.5N was sufficient to achieve good results.

Table 3.4: Initial test pile properties

Pile	$P_{outside}$ (N)	W_{pile} (N)	W_{plug} (N)	T_{ULT} with plug (N)	T_{ULT} no plug (N)
900 x 18 x 3mm acrylic	66.3	1.8	1.4	69.5	68.1

3.3.2. Pile improvements

Pull-out tests were carried out to ascertain the true ultimate capacity of the pile.

- 1) Bare pile, figure 3.5(a)

Despite original predictions on the order of 69.5N, figure 3.5(a) demonstrates that the true ultimate capacity of the pile was actually around 28N.

The soil-pile friction angle δ - originally predicted to be 15° - might have been lower, because an acrylic surface is likely to be smoother than a steel surface. In order to increase the ultimate capacity of the pile without significant changes to the pile's geometry, and whilst continuing to test at 1g, an attempt was made to increase δ .

2) Glued pile, figure 3.5(b)

To increase δ the pile surface was roughened. Araldite glue was used to glue Hostun sand onto the outside surface of the pile.

In the first pull-out test with the new ‘glued’ pile, a T_{ULT} of 90.5N was achieved. However, on each subsequent pull-out or cycle its ultimate capacity decreased (figure 3.5(b)). This was because the sand on its exterior was gradually being worn away.

The test PO-G-3 shows an ultimate capacity of only 14.2N, a value so low that it cannot be explained by the degradation of the pile surface alone. It is likely the pile was knocked or twisted during installation.

3) Sandpaper pile stage 1, figure 3.5(c)

In order to create a rough surface that would not degrade during installation and loading, P60 was sandpaper glued onto the surface. Throughout all the proceeding tests it showed no signs of degradation. The addition of sandpaper increased the pile’s diameter to 19.2mm, and therefore its length to 950mm (in order to maintain $L/D=50$).

However, as figure 3.5(c) demonstrates, the ultimate capacity of the sandpaper pile was still highly variable. It was deduced that this was due to the installation method, which is discussed in more detail later in this section.

4) Sandpaper pile stage 2, figure 3.5(d)

Rather than driving the pile into the sand as had been happening previously, the pile was held in the centre of the container with a jig and sand was poured around it.

Consistency was finally achieved, with an average ultimate capacity, T_{ULT} , of $125.2 \pm 15.5N$ ($125.2N \pm 19\%$). Not only was this ultimate capacity relatively consistent, it was also very high, which helped to improve the SNR of the proceeding cyclic tests.

The updated pile properties are presented in table 3.5. By assuming that the soil-pile friction angle δ remains at of 15° , the method predicts the test pile to have an ultimate capacity of only 80.3N. However, due to the sandpaper δ is likely to be greater than 15° , and this can explain the discrepancy.

Table 3.5: Final test pile properties

Pile	T_{ULT} predicted (N)	T_{ULT} actual (N)
950 x 19.2 x 3mm acrylic covered with P60 sandpaper	80.3	125.2

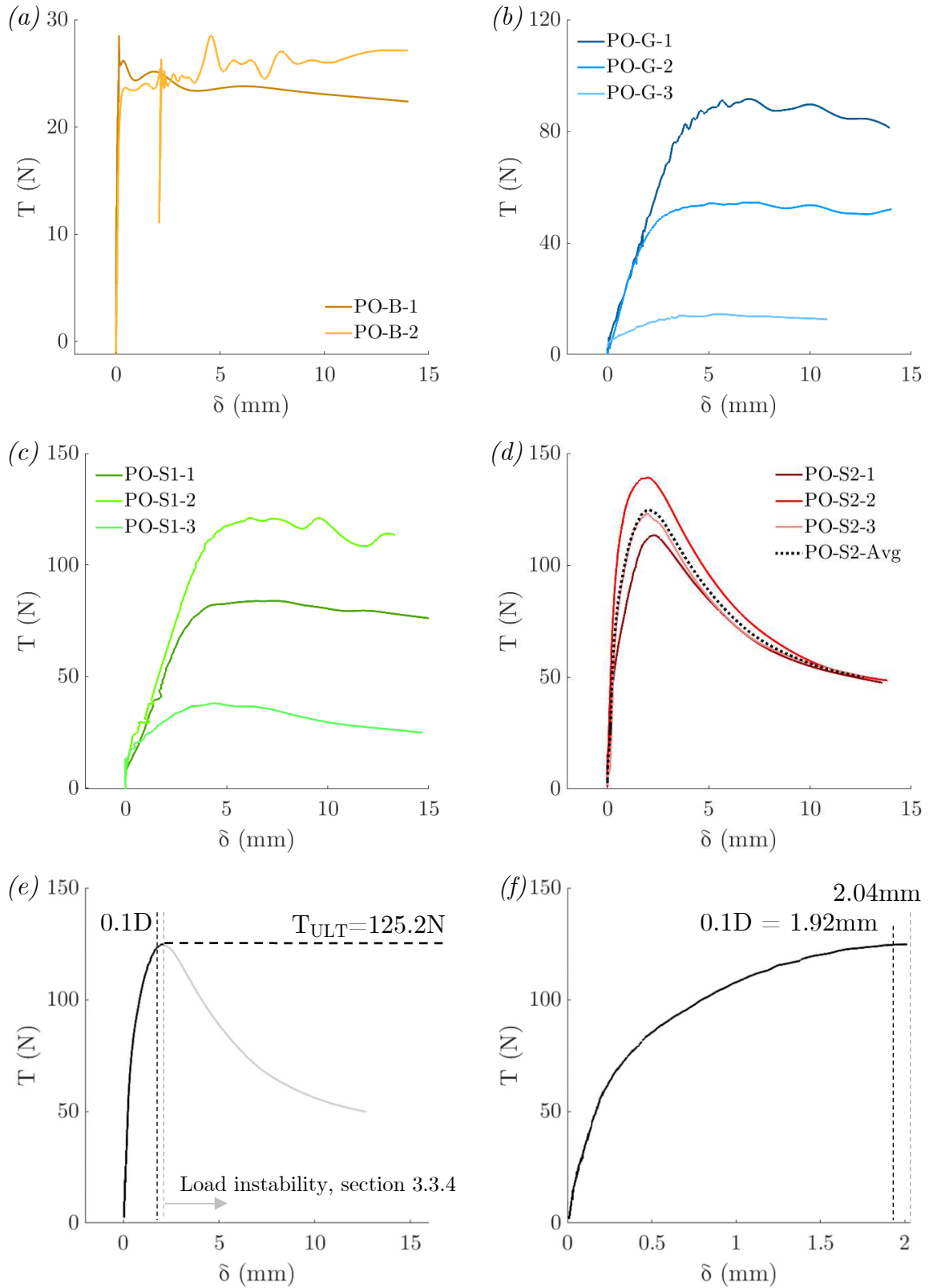


Figure 3.5: (a) 2 pull-out tests on bare pile, average $T_{ULT} = 27.0N \pm 0.7\%$
 (b) 3 pull-out tests on glued pile, average $T_{ULT} = 38.8N \pm 73\%$
 (c) 3 pull-out tests on sandpaper pile stage 1, average $T_{ULT} = 80.8N \pm 53\%$
 (d) 3 pull-out tests on sandpaper pile stage 2, average $T_{ULT} = 125.2N \pm 19\%$
 (e) PO-S2-Avg showing load instability, (f) PO-S2-Avg zoomed in to peak

3.3.3. Installation method

Originally, the pile was installed using a template to hold it vertically in the centre of the container whilst a rubber mallet was used to drive it gently into the sand. Consistency between tests was achieved by ensuring that the number of blows taken to drive the pile every 10cm of its length was be replicated across all tests.

It was assumed that the installation process would have very little effect on the results of the tests. However, it was found that despite the best attempts to achieve consistency, the ultimate capacity of the test pile was highly sensitive to the installation process. The reason for this is likely that the horizontal stress acting on the pile shaft was more strongly influenced by the number of installation cycles than had been expected (White & Lehane, 2004).

Therefore, instead of driving the pile, the pile was held in the centre of the container with a jig and the sand was poured around it (figure 3.6). The sand did not experience any stresses during the test's set up, and therefore behaved consistently for each test.



Figure 3.6: Jig holding the pile, whilst sand is poured around it

3.3.4. Load instability

For tests PO-S2, after the peak load T_{ULT} had been reached at 2.04mm (figure 3.5(f)), the force applied to the pile dropped suddenly. This is due to the pile pulling upwards out of the ground faster than the mass on the lever arm is able to move down. This caused a sudden reduction in the cable tension (figure 3.5(e)).

Therefore, after the peak, the pull-out test is no longer load-controlled, and the data recorded by the loadcell should be discounted. A horizontal dashed line has been drawn at T_{ULT} , and a vertical line at $0.1D$, for reference.

4. Results and Discussions

4.1. Pull-out capacity

4.1.1. Comparison of PO-S1 and PO-S2

Pouring the sand around the pile (PO-S2), instead of driving the pile into the sand (PO-S1), increased the average ultimate capacity of the pile, T_{ULT} , from 80.8N to 125.2N and the average initial stiffness, k_{Avg} , from 26Nmm⁻¹ to 210Nmm⁻¹.

The difference in strength and stiffness is due to “friction fatigue”. In general, when a pile is driven into sand, shearing at the soil-pile interface causes the sand around the pile to densify. This leads to stress relief and therefore a decrease in the shaft friction along the pile (White & Bolton, 2004), resulting in a lower strength and stiffness. When instead, sand is simply poured around the outside of the pile, there is no degraded surface around the outside of the pile, and the full shear strength and stiffness of the sand is mobilised. Therefore, the stress history of the sand following installation has a large effect on the response of the pile, though this is not the focus of this report.

4.2. Cyclic response

4.2.1. Applied loading

Table 4.1 details the loads applied during the cyclic tests. The rig was able to apply consistent cyclic loading for the duration of each test, with only a $\pm 2N$ variation in T_{MIN} and T_{MAX} . The values of T_{CYC}/T_{MAX} and T_{MAX}/T_{ULT} achieved are close to the target values detailed in table 2.7, but not exactly the same. This was due to experimental errors setting up the test rig, and friction in the system.

Table 4.1: Applied cyclic loading

Test	T_{CYC}/T_{MAX} Load case		T_{MAX}/T_{ULT} Safety factor		T_{CYC}/T_{ULT}	T_{MEAN}/T_{ULT}	T_{MAX}/T_{ULT} ζ_b	T_{MIN}/T_{MAX} ζ_c	Total applied cycles
	Target	Actual	Target	Actual					
CYC-E-1.5	0.4	0.37	1.5	1.39	0.27	0.46	0.73	0.26	55
CYC-E-2.25	0.4	0.40	2.25	1.93	0.21	0.32	0.53	0.20	356
CYC-N-1.5	0.2	0.22	1.5	1.46	0.16	0.54	0.70	0.55	189
CYC-N-2.25	0.2	0.20	2.25	2.14	0.09	0.37	0.47	0.59	8037
CYC-N-3	0.2	0.21	3	2.58	0.08	0.31	0.39	0.59	8556

Other relevant force ratios are included in table 4.1 for reference. $T_{\text{CYC}}/T_{\text{ULT}}$ and $T_{\text{MEAN}}/T_{\text{ULT}}$ are used in interaction diagrams (e.g. section 4.2.4, figure 4.8), and ζ_b and ζ_c are commonly used to describe the lateral loading of piles (Leblanc, et al., 2010a).

Figure 4.1 shows the typical results obtained for each cyclic test. Of particular interest are the T - δ (figure 4.1(b)) and δ - N (figure 4.1(c)) curves, which are shown for all five cyclic tests in figures 4.2 and 4.4 respectively.

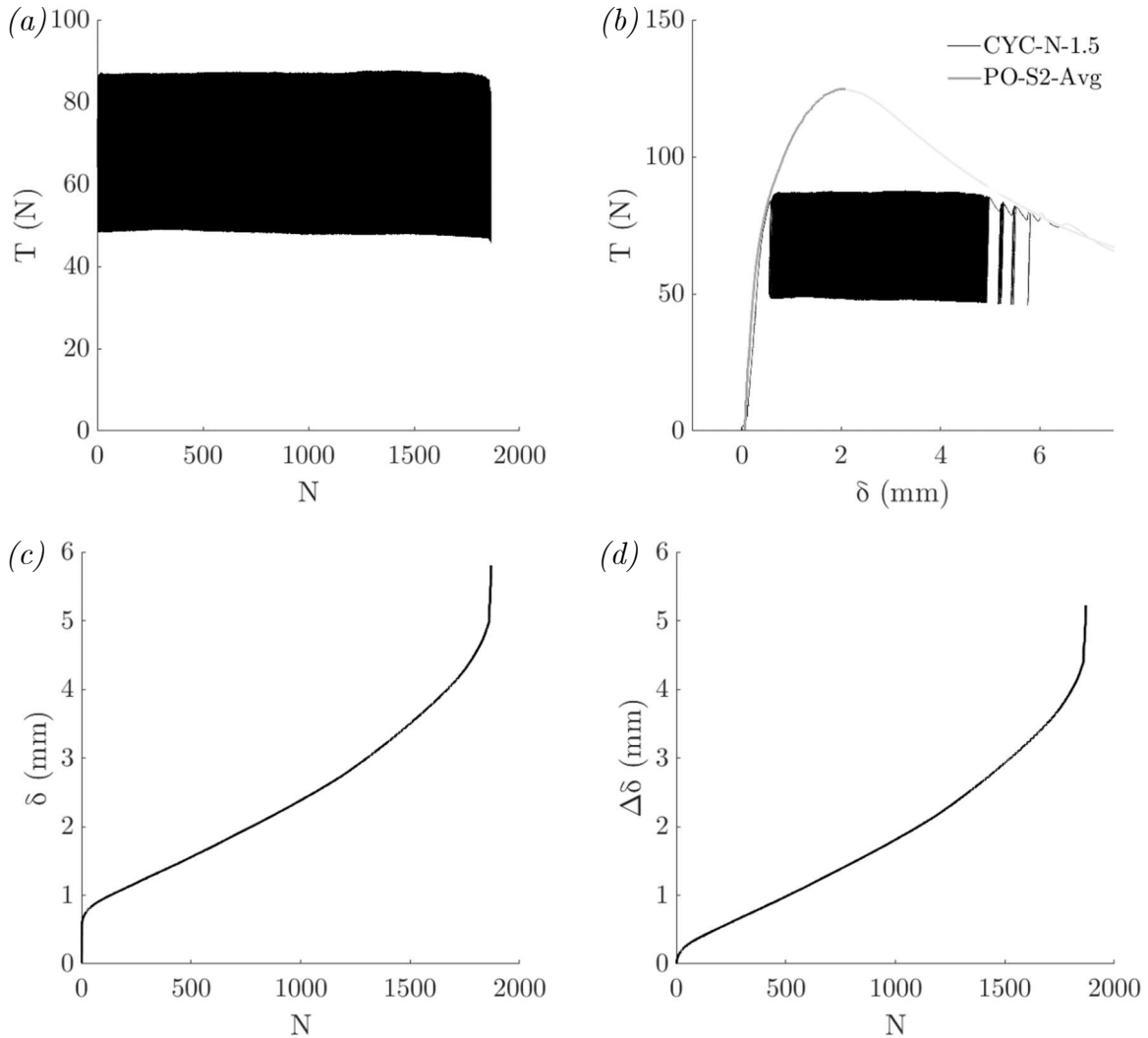


Figure 4.1: CYC-N-1.5 results (a) T - N , (b) T - δ , (c) δ - N , (d) $\Delta\delta$ - N

Figure 4.2 clearly shows the five combinations of $T_{\text{CYC}}/T_{\text{MAX}}$ and $T_{\text{MAX}}/T_{\text{ULT}}$ applied to each pile. As expected, the monotonic response of each pile follows the curve of PO-S2-Avg. The load begins to cycle, causing the piles to displace at different rates. In the stable and meta-stable tests, displacement continues until the pile can no longer sustain T_{MAX} and the pile pulls out of the sand, experiencing load instability similar to that of PO-S2-Avg (section 3.3.4).

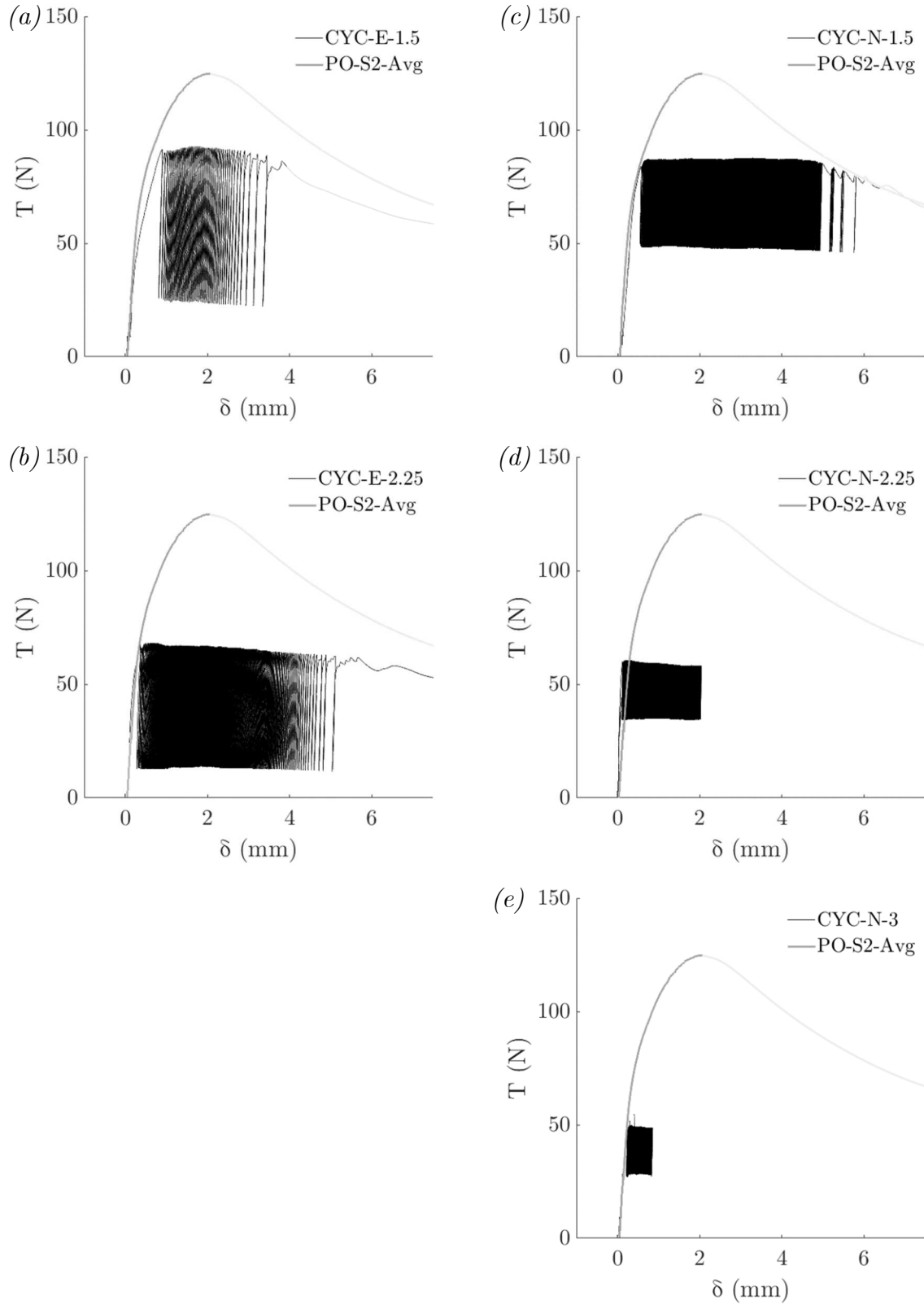


Figure 4.2: T - δ curves with $PO-S2-Avg$ for reference
 (a) $CYC-E-1.5$: unstable, (b) $CYC-E-2.25$: meta-stable,
 (c) $CYC-N-1.5$: meta-stable, (d) $CYC-N-2.25$: stable, (e) $CYC-N-3$: stable

4.2.2. Pile displacement

The displacement of the piles due to cyclic loading can be characterised by the four cycle numbers defined below and shown in figure 4.3(a).

- N_i is the point of inflexion, after which the second derivative of the δ -N curve becomes positive.
- $N_{0.1D}$ is the point at which the pile has displaced 0.1D, 1.92mm. Whichever occurs first of $N_{0.1D}$ or N_f determines whether the test is stable, meta-stable or unstable (section 2.4.1).
- N_a is the ‘point of acceleration’ after which the pile begins to show a noticeable increase in displacement rate. This has potential use for TLP designers, as it signals impending shaft failure. It has been defined using the empirical displacement law (section 4.2.3), as the point at which the $\log(\Delta\delta/\delta_s)$ - $\log(N)$ curve of each cyclic test crosses above its trend line (figure 4.3(b)). δ_s is the displacement of the pile that would occur in a static test if the load were equivalent to the maximum cyclic load T_{MAX} (shown in figure 4.3(a)).
- N_f is the point of shaft failure after which the pile can no longer sustain T_{MAX} and it accelerates rapidly.

Table 4.2. records the cycle numbers for each of the five cyclic tests.

Table 4.2: Cyclic loading results

Test	N_i	$N_{0.1D}$	N_a	N_f	Response
CYC-E-1.5	20	31	38	55	Unstable
CYC-E-2.25	130	168	280	356	Meta-stable
CYC-N-1.5	330	717	1103	1869	Meta-stable
CYC-N-2.25	>8037	7037	n/a	>8037	Stable
CYC-N-3	>8556	>8556	n/a	>8556	Stable

Figure 4.4. shows the δ/D -N curves for each of the five cyclic tests and typical stable, meta-stable and unstable behaviour. Tests CYC-N-3 and CYC-N-2.25 behaved in a stable manner and therefore, due to time restrictions, it was not possible to run them until shaft failure (Appendix B). Instead, they ran for 8037 and 8556 cycles respectively before the motor was stopped and pull-out tests was carried out (PO-CYC-N-3 and PO-CYC-N-2.25, discussed in section 4.2.4).

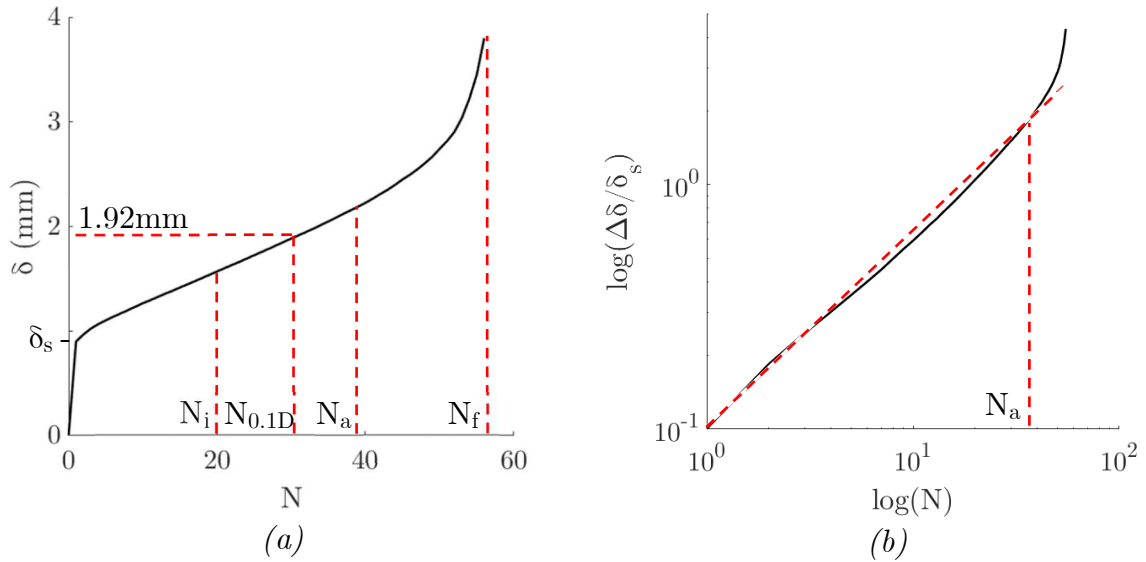


Figure 4.3: CYC-E-1.5, (a) N_i , $N_{0.1D}$, N_a and N_f marked, (b) definition of N_a

These results can also be used to determine the suitability of the ABS safety factors for TLP driven pile anchors.

The CYC-E-2.25 test behaved in a meta-stable manner failing after only 168 cycles. The safety factor for extreme loading, 2.25, is therefore insufficient and unsafe, as it implies that during extreme loading such as a storm, the TLP's pile would fail after only 168 cycles. The author acknowledges that the actual safety factor applied to the pile was 1.93 (table 4.1) but expects that an actual safety factor of 2.25 would still have resulted in meta-stable behaviour, as predicted by equation 18, discussed below.

On the other hand, the safety factor for normal loading, 3, is potentially sufficient for a safe design. This is because the behaviour of test CYC-N-3 is stable, sustaining over 8556 cycles (despite the actual safety factor during the test being lower, 2.58 (table 4.1)). Figure 4.5(e) demonstrates this stable behaviour, as the displacement rate decelerates and begins to stabilise.

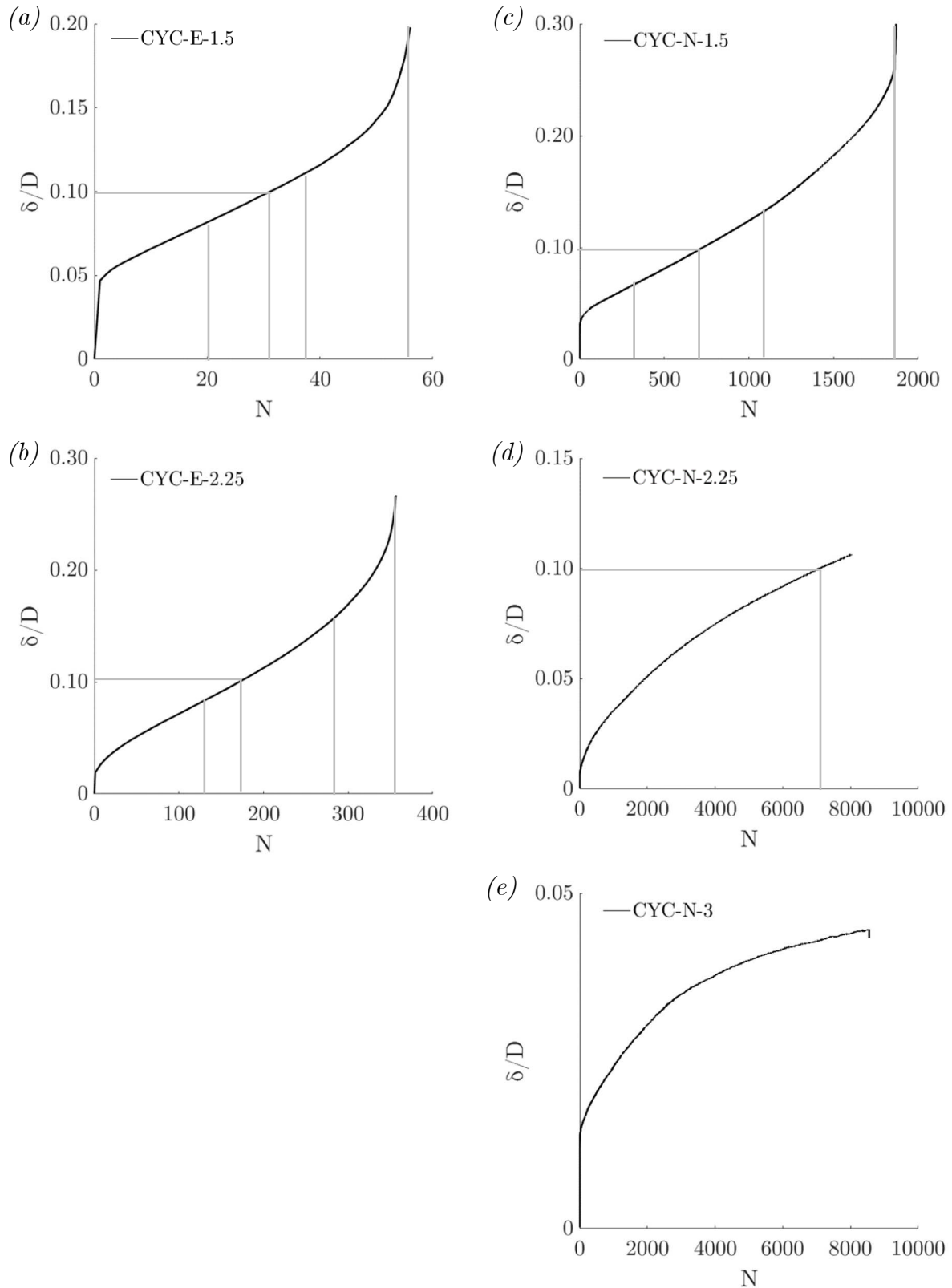
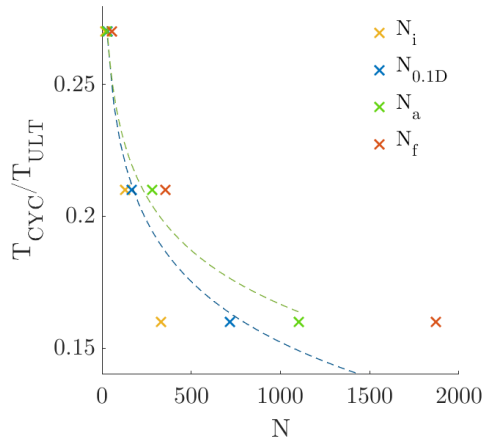


Figure 4.4: δ/D - N curves with N_i , $N_{0.1D}$, N_a and N_f marked
 (a) CYC-E-1.5: unstable, (b) CYC-E-2.25: meta-stable,
 (c) CYC-N-1.5: meta-stable, (d) CYC-N-2.25: stable, (e) CYC-N-3: stable

The results in table 4.2 clearly show that an increase in the amplitude of cyclic loading T_{CYC}/T_{MAX} , or a decrease in the safety factor T_{ULT}/T_{MAX} , both have a detrimental effect on the number of cycles that a pile can sustain.

An investigation was made into whether there was a single force ratio that controlled the cycle number of a pile. All the force ratios in table 4.1 were considered. It was found that T_{CYC}/T_{ULT} (the combination of T_{CYC}/T_{MAX} and T_{MAX}/T_{ULT}) was the only force ratio that showed a correlation with the cycle numbers (figure 4.5). This suggests that for the most part, the response of a pile is controlled by T_{CYC}/T_{ULT} . This is consistent with empirical degradation law, in which T_{CYC}/T_{ULT} was sufficient to predict a pile's cyclic degradation (section 2.4.2) (Jardine & Standing, 2012).

Equations 18 and 19 show the logarithmic laws fit to figure 4.5 for cycle numbers $N_{0.1D}$ and N_a respectively.



$$\frac{T_{CYC}}{T_{ULT}} = -0.033 \times \ln(N_{0.1D} \times 10^{-5}) \quad (18)$$

$$\frac{T_{CYC}}{T_{ULT}} = -0.030 \times \ln(N_a \times 3.5 \times 10^{-6}) \quad (19)$$

Figure 4.5: $N_{0.1D}$ and N_a fits

Equation 18 can be used to calculate the value of T_{CYC}/T_{ULT} for which cyclic tests should behave in a stable manner. By inputting $N_{0.1D}=1000$, the resulting T_{CYC}/T_{ULT} is 0.152 for stable loading. This corresponds to a safety factor of 1.32 for the normal load case (for which $T_{CYC}/T_{MAX}=0.2$), and 2.63 for the extreme load case (for which $T_{CYC}/T_{MAX}=0.4$). The latter number suggests that the safety factor recommended by ABS design guidelines for extreme loading (2.25) is unsafe, since the pile requires a safety factor of at least 2.63 to behave in a stable manner.

Equation 19 could be used by designers to ensure that N_a cycles do not occur within the TLP's lifetime, and therefore that the anchor will never reach a point at which it loses stability and accelerates. To account for the variety of loading experienced by the pile, a 'cumulative damage' approach to design can be taken (discussed in section 4.2.6).

4.2.3. Displacement law

An empirical law like that of equation 9 (section 2.4.3) for the rotation of laterally loaded piles after N cycles, was desired for the displacement of axially loaded piles.

Several different fits were attempted, including a logarithmic fit, but the resulting empirical power laws shown in equations 20 and 21 were the most successful. It was found that the fits were better when stable tests were treated separately to unstable and meta-stable tests, and when the fit for stable tests considered long term loading only (after 200 cycles). The equations are similar in form to equation 9.

$$\frac{\Delta\delta}{\delta_s} = a N^{0.81} \quad \text{for unstable and meta-stable response} \quad (20)$$

$$\frac{\Delta\delta}{\delta_s} = d N^{0.55} \quad (\text{after 200 cycles}) \text{ for stable response} \quad (21)$$

a and d are dimensionless equations, studied in figure 4.6(a) and 4.6(b) respectively.

After testing several different force ratios it was found that the variable a was a function of T_{CYC}/T_{ULT} . This was to be expected since for the most part T_{CYC}/T_{ULT} controls the pile's displacement (section 0) and degradation (section 4.2.4). The function is shown in figure 4.6(a), and the updated law is shown in equation 22.

$$\frac{\Delta\delta}{\delta_s} = 5.3 \left(\frac{T_{CYC}}{T_{ULT}} \right)^{3.0} N^{0.81} \quad (22)$$

It was not possible to find an equivalent fit for d since there were not a sufficient number of data points (stable tests) to produce a curve (figure 4.6(b)).

Figure 4.8(a) shows the $\Delta\delta/\delta_s$ - N curves for the five cyclic tests, and figure 4.8(b) shows the two empirical displacements laws of equation 21 and equation 22, plotted on $\log(\Delta\delta/\delta_s)$ - $\log(N)$ axes. The fits are good, suggesting these laws can be used to predict the displacement of the piles. However, in the cases of the unstable and meta-stable tests, the law does not fit well once the pile displacement begins to accelerate. These are the points defined as N_a , shown by the vertical dotted lines on figure 4.8(b).

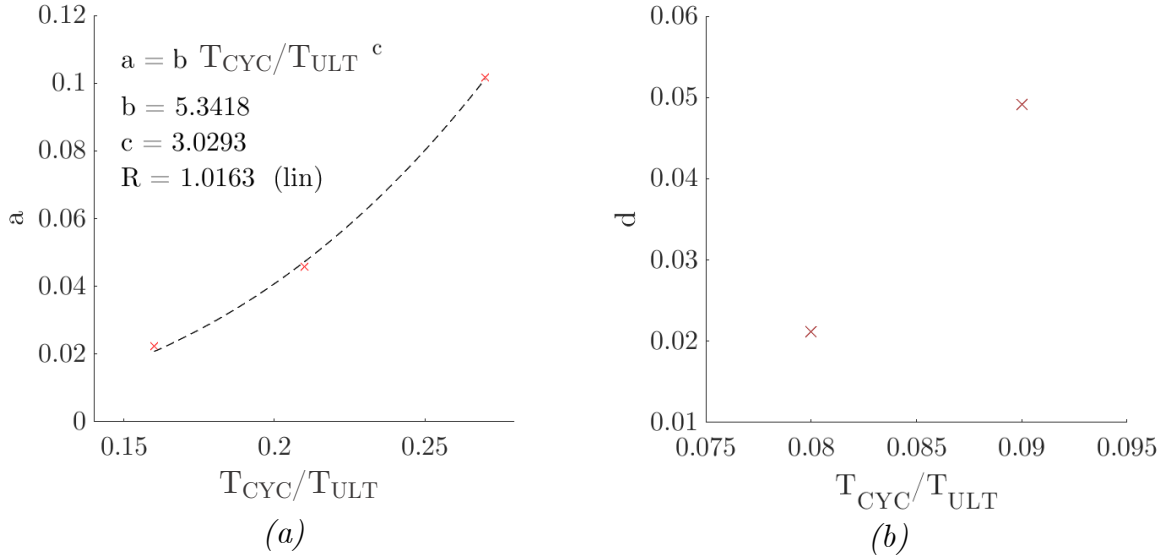


Figure 4.6: (a) $a-T_{CYC}/T_{ULT}$, including fit, (b) $d-T_{CYC}/T_{ULT}$

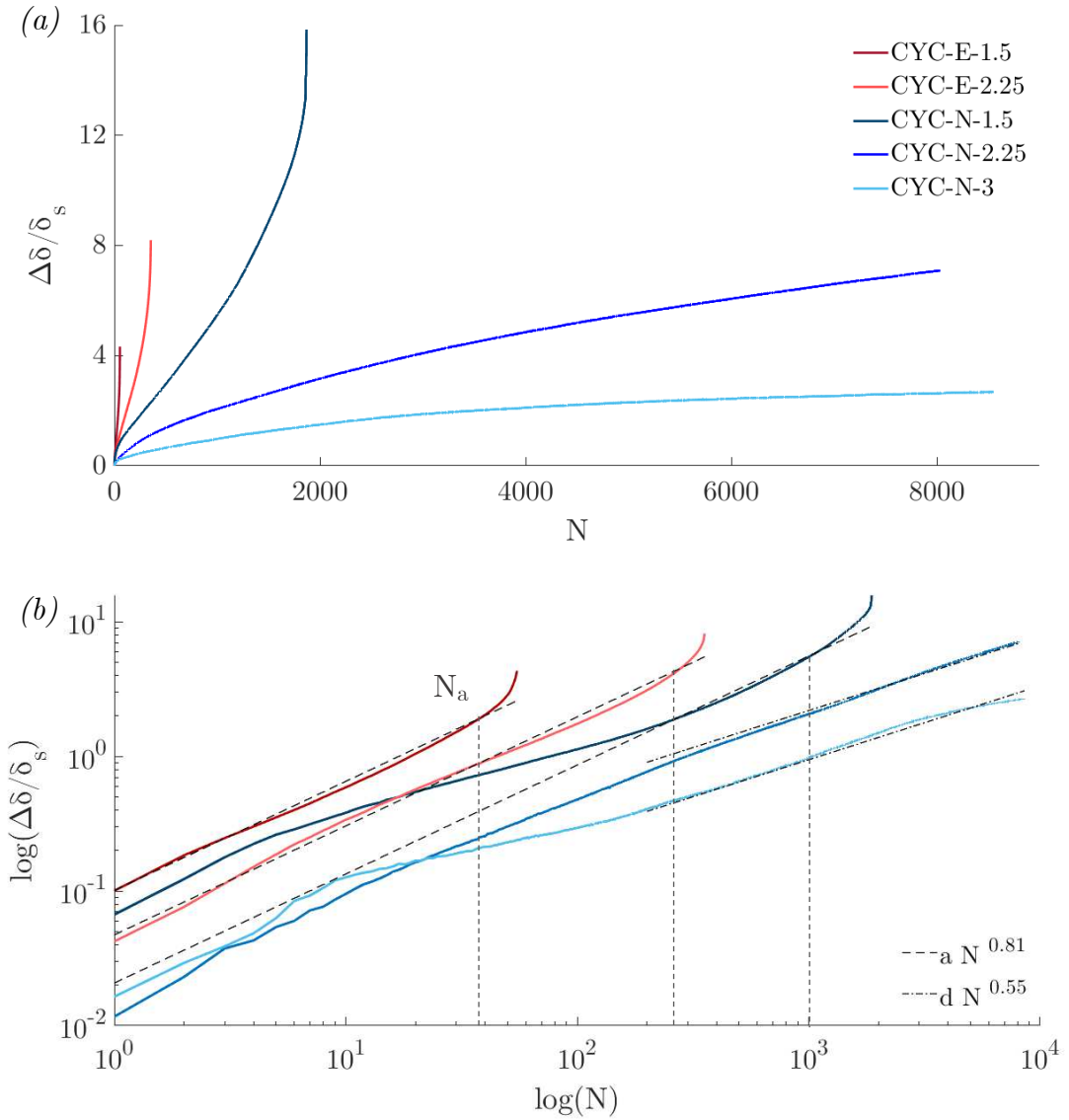


Figure 4.7: (a) $\Delta\delta/\delta_s-N$ curves, (b) $\log(\Delta\delta/\delta_s)-\log(N)$ curves, including fits

4.2.4. Interaction diagram

The cyclic test results were plotted on Jardine and Standing's interaction diagram for the tensile cyclic loading of open-ended piles in Dunkirk Sand (Jardine & Standing, 2012).

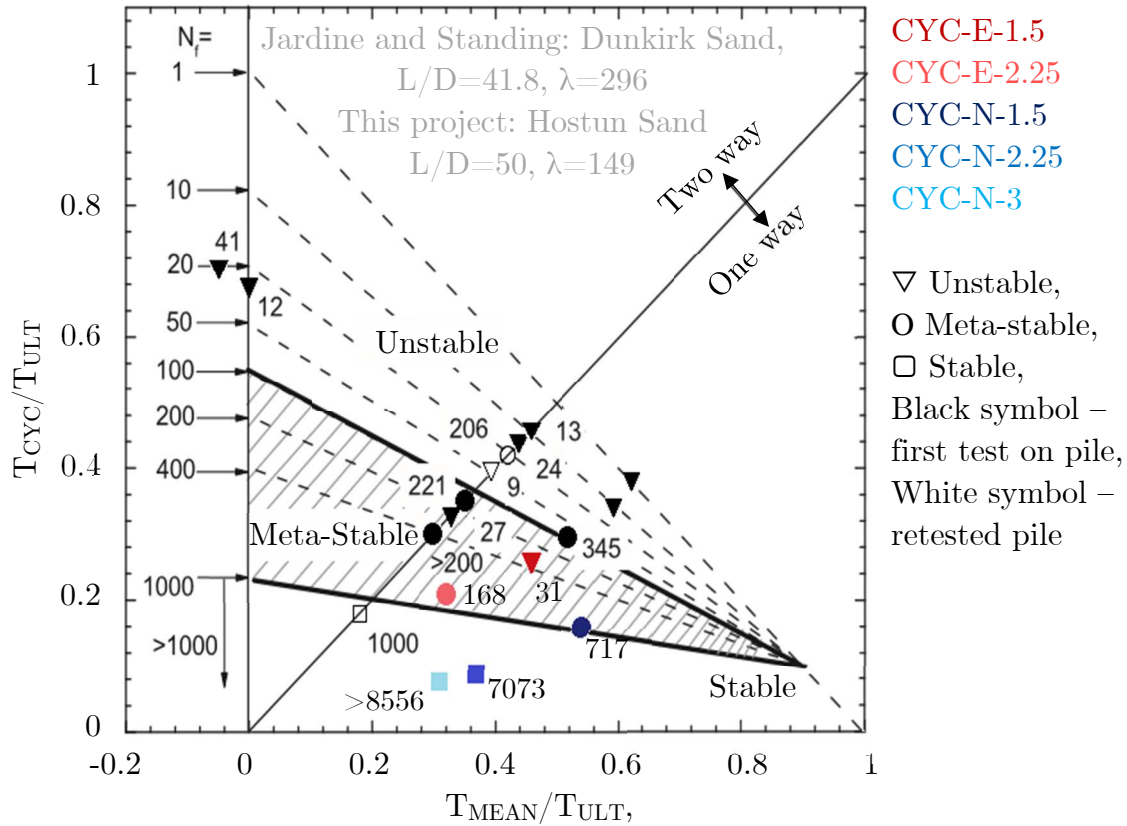


Figure 4.8: Interaction diagram, with cyclic test results added

The number of cycles labelled on figure 4.8 are $N_{0.1D}$, as during this project's cyclic tests the pile displaced $0.1D$ before shaft failure occurred. Jardine and Standing's piles however, generally experienced shaft failure before they reached a displacement of $0.1D$.

Figure 4.8 shows that the cyclic test results show good agreement with the Jardine and Standing interaction diagram. The interaction diagram correctly predicts the stable, meta-stable or unstable behaviour of all but one cyclic test.

That one cyclic test is CYC-E-1.5, which experienced unstable behaviour despite the interaction diagram predicting it would be meta-stable. The interaction diagram also overpredicts the number of cycles required to fail the other 'extreme' test – CYC-E-2.25. Since the Jardine and Standing interaction diagram over-predicts the number of cycles to failure for these tests, it suggests that as a design tool it is not conservative and that it is therefore unsafe.

However, the exact zones and cycle numbers are likely to vary with soil conditions and pile parameters (Tsuha, et al., 2012). Despite both sets of results having similar scaling ($L/D=50$, $\lambda=149$ in this project and $L/D=41.8$, $\lambda=296$ in Jardine and Standing's), the tests are not exactly equivalent. Therefore, in order for TLP driven pile anchor designers to achieve accurate cycle numbers using an interaction diagram, results are needed which scale precisely with the relevant pile parameters and soil conditions of their design.

4.2.5. Cyclic degradation

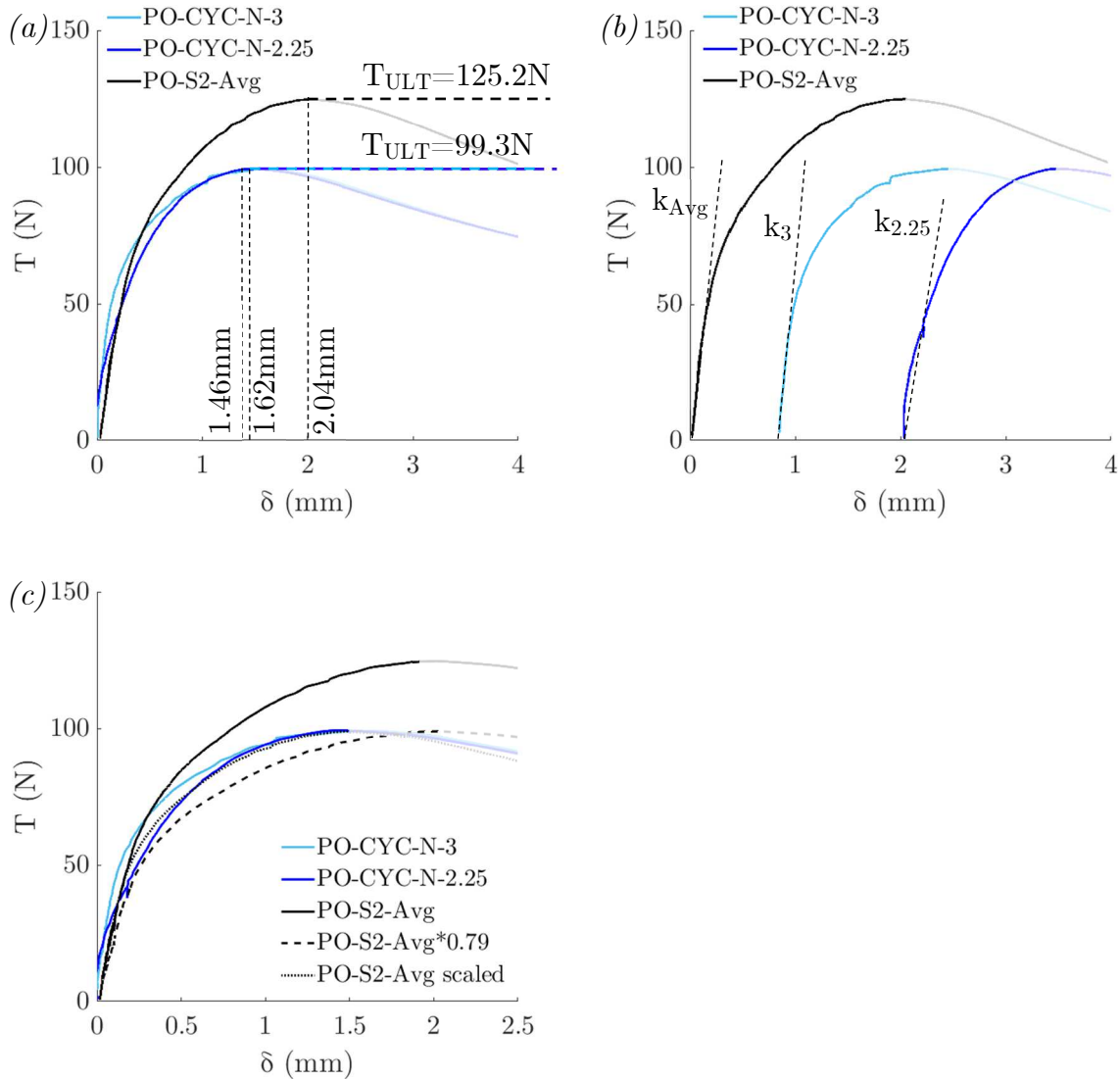


Figure 4.9: Pull-out tests after stable cyclic loading, (a) T - δ curve. Displacements at peak marked, (b) T - δ curve displaced by δ_{ref} , the displacement of each pile achieved during the preceding cyclic loading. Stiffnesses k_{Avg} , k_3 and $k_{2.25}$ marked, (c) PO-S2-Avg scaled to match the curves.

Figure 4.9(a) shows the pull-out tests carried on CYC-N-3 and CYC-N-2.25 once they had been stopped early. In both tests T_{ULT} degraded from 127.3 to 99.3N, a 21% reduction in strength (figure 4.9(c)). This behaviour is unlike the stable tests observed by Tsuha, Jardine and Standing, in which the strength of the pile increased (Tsuha, et al., 2012; Jardine & Standing, 2012). This suggests the safety factors of 2.25 or 3 are not safe for use with normal load cases, as they cause the strength of the pile to degrade.

The initial stiffness, k , of each pull-out test was also measured. Achieving a precise value of stiffness was difficult – particularly due to noise in the signals. However, values of $k_{Avg}=210\text{Nmm}^{-1}$, $k_3=300\text{Nmm}^{-1}$ and $k_{2.25}=180\text{Nmm}^{-1}$ were measured (figure 4.9(b)). Therefore, the test CYC-N-2.25 caused a slight decrease in pile stiffness but CYC-N-3 generated a significant increase. Further tests are required in order to draw a conclusion on the effect of cyclic loading on the initial stiffness of the pile.

The resulting T - δ curves are remarkably similar in shape to each other, and to the original pull-out. This is illustrated in figure 4.9(c) in which the T - δ curve of PO-S2-Avg is scaled in the x and y axes, so that the three peaks effectively converge.

4.2.6. Degradation law

The degradation of the pile’s ultimate capacity can be predicted using Jardine and Standing’s degradation law (Jardine & Standing, 2012) described in section 2.4.2.

The cyclic test results were used to fit values of A , B and C (equation 23), in order for an interaction diagram to be plotted with lines of constant shaft failure, N_f , like that of figure 2.5(b) (section 2.4.2).

$$\frac{\Delta T_{ULT}}{T_{ULT}} = A \left(B + \frac{T_{CYC}}{T_{ULT}} \right) N^C \quad (23)$$

For the cyclic tests which experienced shaft failure, the reduction in their ultimate capacity ΔT_{ULT} was taken as $T_{MAX}-T_{ULT}$. For the two stable tests which did not experience shaft failure, their ultimate capacity dropped to 99.3N (section 4.2.4).

Table 4.3 : Values used to fit A , B and C

Test	ΔT_{ULT} (N)	$\Delta T_{ULT}/T_{ULT}$	T_{CYC}/T_{ULT}	N_f
CYC-E-1.5	-33.6	-0.27	0.27	55
CYC-E-2.25	-59.0	-0.47	0.21	356
CYC-N-1.5	-38.1	-0.30	0.16	1869
CYC-N-2.25	-25.9	-0.21	0.09	>8556
CYC-N-3	-25.9	-0.21	0.08	>8037

A, B and C were found by linear regression. The coordinates of the five cyclic tests in table 4.3 were plotted on $\Delta T_{ULT}/T_{ULT}$ vs T_{CYC}/T_{ULT} axes, as were lines of equation 23 for the five values of N_f . The square of the distance was measured between the line and its corresponding coordinate for different values of A, B and C. These squared distances were added together, and the minimum was found.

This minimum corresponds to the values $A=-0.26$, $B=-0.08$ and $C=0.43$.

$$\frac{T_{CYC}}{T_{ULT}} = \frac{\frac{T_{MEAN}}{T_{ULT}} - 1 - 0.26 * 0.08 * N_f^{0.43}}{-0.26 * N_f^{0.43} - 1}} \quad (24)$$

Equation 24 (derived from equation 8 and the values of A, B and C) was used to plot the shaft failure interaction diagram shown in figure 4.10(a).

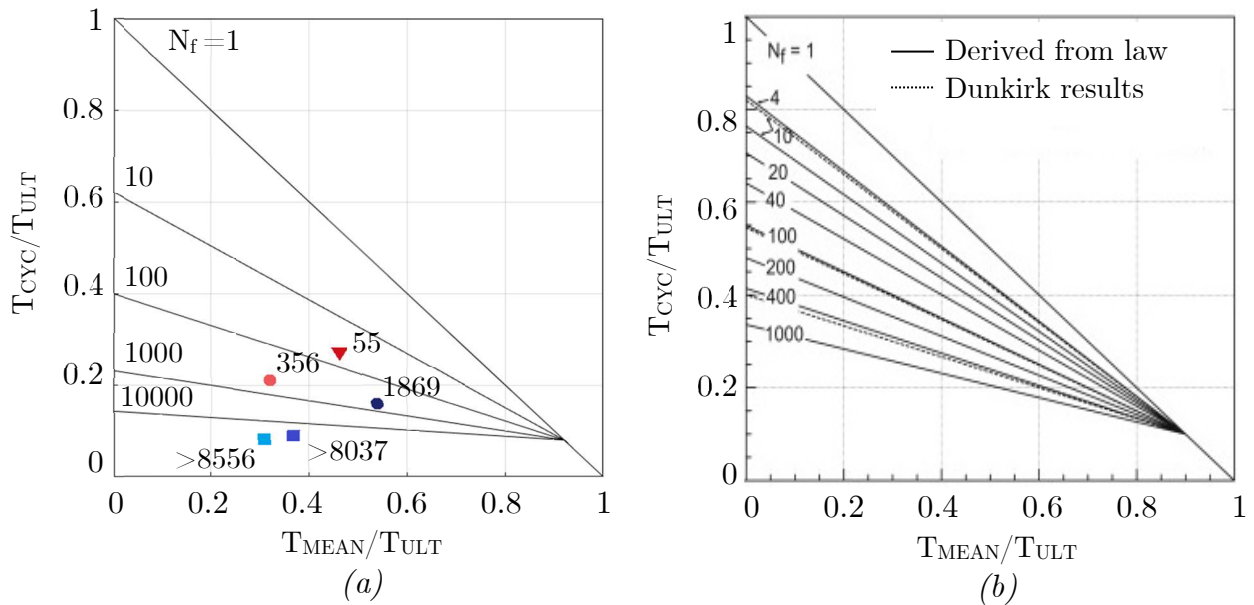


Figure 4.10: Shaft failure interaction diagram, (a) $A=-0.26$, $B=-0.08$, $C=0.43$
 (b): (Jardine & Standing, 2012) $A=-0.126$, $B=-0.10$, $C=0.45$

The plot matches well with Jardine and Standing's (4.10(b)) since the constants A, B and C are similar. However, like in the interaction diagram of figure 4.8, Jardine and Standing's plot predicts failure at a greater number of cycles for any given load. Again, this discrepancy can likely be explained by the fact that the tests are not exactly equivalent.

By using $B=-0.08$ in equation 23, $\Delta T_{ULT}/T_{ULT}=0$ when $T_{CYC}/T_{ULT}=0.08$. Therefore, the empirical degradation law predicts that as long as $T_{CYC}/T_{ULT}<0.08$, no cyclic degradation of the pile's ultimate capacity will occur.

For ‘normal’ load cases in which $T_{CYC}/T_{MAX}=0.2$, for T_{CYC}/T_{ULT} to be less than 0.08, a safety factor of $T_{ULT}/T_{MAX}=2.5$ is required. This is less than the safety factor recommended by the ABS design guidelines, 3, suggesting that the ABS recommendation is safe. However, it is also less than the safety factor applied to the test CYC-N-3, which did experience ultimate capacity degradation. This suggests a limit to the accuracy with which the empirical degradation law can predict the reduction in a pile’s ultimate capacity.

For ‘extreme’ load cases in which $T_{CYC}/T_{MAX}=0.4$, for T_{CYC}/T_{ULT} to be less than 0.08, a safety factor of $T_{ULT}/T_{MAX}=5$ is required. This is far greater than the safety factor of 2.25 recommended for extreme loading in the ABS guidelines. However, achieving such a safety factor is unlikely to be practical, as the material usage and associated costs for such a large pile would be significant.

A solution to this problem is to use a ‘cumulative damage’ approach to design. Over the lifetime of a TLP driven pile anchor, the tension signal on its anchors can be “grouped into batches of cycles with constant amplitudes” (Jardine & Standing, 2012). Each of these batches of N cycles causes damage (cyclic degradation) to the pile, the value of which can be predicted using the empirical degradation law in equation 25.

Safety factors can be set such that damage accumulates slowly and does not cause the anchor to fail within its 20-year lifetime. The appropriate safety factors will ensure the pile does not experience damage during ‘normal’ loading conditions, but is allowed to accumulate small amounts of damage during extreme loading conditions.

$$\frac{\Delta T_{ULT}}{T_{ULT}} = -0.26 \left(-0.08 + \frac{T_{CYC}}{T_{ULT}} \right) N^{0.43} \quad (25)$$

5. Conclusions

The pull-out and cyclic loading tests detailed in this report lead to the following conclusions. These are useful for the design of driven pile anchors for TLPs and provide an insight into the cyclic axial loading of piles in sand in general.

- The installation method has a strong effect on the ultimate capacity achieved by the test pile, and its variability. This was because, when driving the pile, the sand experienced friction fatigue, a phenomenon that was not present when the sand was poured around the pile.
- The safety factor of 2.25 for extreme loading recommended by the ABS design guidelines is insufficient, as the cyclic test experienced meta-stable behaviour.
- The safety factor of 3 for normal loading recommended by the ABS design guidelines is potentially sufficient, as the cyclic test experienced stable behaviour. However, unlike in other results from published literature, this was not matched by an increase in the pile's ultimate capacity.
- The main driver of the pile's response to cyclic loading was T_{CYC}/T_{ULT} , a combination of the safety factor, T_{ULT}/T_{MAX} , and load case, T_{CYC}/T_{MAX} . An increase in T_{CYC}/T_{ULT} caused cyclic degradation to occur faster and therefore the number of cycles to failure to decrease.
- The value of T_{CYC}/T_{ULT} required to achieve a certain number of cycles to a displacement of $0.1D$, $N_{0.1D}$, or to the 'point of acceleration', N_a , can be predicted with an empirical logarithmic law.
- The displacement of the pile due to N cycles of cyclic loading can be predicted using an empirical power law for design.
- The cyclic tests were plotted on Jardine and Standing's interaction diagram and showed consistency with the existing results.
- Jardine and Standing's empirical degradation law was fitted to the cyclic test results and the corresponding interaction diagram with lines of constant N_f was plotted. This diagram can be used to predict the number of cycles to shaft failure, for different load combinations. It can also be used to predict the cyclic degradation experienced by a pile, so that a 'cumulative damage' approach to design can be used.

Several recommendations for further study are identified below, some of which could not be achieved by the author due to the COVID-19 outbreak.

- During the pull-out tests, load-control was lost after the load reached its peak, and therefore the results beyond this point are not suitable for detailed analysis. This is a limitation of the project since the behaviour of the pile after the peak is important in explaining the behaviour of the sand as the pile is pulled out. The author recommends carrying out further tests in which, rather than using the cyclic test rig's lever arm to apply load to the pile, load is applied, for example, by the incremental addition of masses.
- There are further cyclic tests that could be carried out, in no particular order:
 - 1) further 'extreme' load case tests at greater safety factors, to determine a safety factor at which the pile is stable under extreme loading.
 - 2) further 'normal' load case tests at greater safety factors, to determine a load combination at which the ultimate capacity of the pile increases.
 - 3) further stable tests, so that d as a function of T_{CYC}/T_{MAX} can be determined for use with the empirical displacement law.
- The tests CYC-N-3 and CYC-N-2.25 had to be stopped prematurely. These should be repeated and run until shaft failure, in order to fully determine their behaviour.
- Piles in the field may show different behaviours to the test pile used in this project, in particular due to the low confining stress and relative density at which these tests were performed. It would therefore be interesting to perform the tests at higher confining stresses, for example by using the Schofield Centre centrifuge.

6. Acknowledgements

Firstly, I would like to thank my supervisor, Dr Christelle Abadie, for her generosity in giving me her time, guidance and expertise.

Secondly, I would like to thank the technicians and staff at the Schofield Centre without whom I would not have a project to speak of, in particular John Chandler, Kristian Pether, Mark Smith, Chris McGinnie, David Layfield and Magdalena Charytoniuk.

Finally, I would like to thank my family and friends for their support throughout my time in Cambridge.

7. References

- Abadie, C., 2015. *Cyclic Lateral Loading of Monopile Foundations in Cohesionless Soils*, Oxford: University of Oxford.
- ABS, 2012. *Floating Wind Turbines*, Houston: American Bureau of Shipping (ABS).
- ABS, 2013. *Offshore Anchor Data for Preliminary Design of Anchors of Floating Offshore Wind Turbines*, Houston: American Bureau of Shipping (ABS).
- Achmus, M., Abdel-Rahman, K. & Peralta, P., 2005. *On the design of monopile foundations with respect to static and quasi-static cyclic loading*, Hannover: Institute of Soil Mechanics, Foundation Engineering and Waterpower Engineering, University of Hannover .
- Andersen, A. K., Puech, A, A. & Jardine, R. J., 2013. *Cyclic resistant geotechnical design and parameter selection for offshore engineering and other applications*. Paris, ISSMGE Technical Committee TC 209.
- API, 2000. *API-RP-2A: Recommended Practice for Planning, Designing and Constructing Fixed Offshore Platforms*, Washington: API.
- API, 2000. *Recommended Practice for Planning, Designing and Constructing Fixed Offshore Platforms*, D.C.: American Petroleum Institute (API).
- API, 2010. *Planning, Designing and Constructing Tension Leg Platforms*, D.C.: American Petroleum Institute (API).
- Bachynski, E. & Moan, T., 2012. Design considerations for tension leg platform wind turbines. *Marine Structures*, 29(1), pp. 89-114.
- BEIS, 2020. *Offshore wind Sector Deal*. [Online]
Available at: <https://www.gov.uk/government/publications/offshore-wind-sector-deal/offshore-wind-sector-deal>
[Accessed 14 May 2020].
- BEIS, 2020. *Renewable electricity capacity and generation (ET 6.1 - quarterly)*, London: BEIS.
- Bolton, M. D., 1986. The strength and dilatancy of sands. *Geotechnique*, 36(1), pp. 65-78.
- Bolton, M. D. et al., 1998. *Guidelines for cone penetration tests in sand*. Tokyo, Centrifuge '98.
- Carbon Brief, 2019. *Analysis: Record-low price for UK offshore wind cheaper than existing gas plants by 2023*. [Online]
Available at: <https://www.carbonbrief.org/analysis-record-low-uk-offshore-wind-cheaper-than-existing-gas-plants-by-2023>
[Accessed 16 May 2020].
- Crozier, A., 2011. *Design and Dynamic Modeling of the Support Structure for a 10 MW Offshore Wind Turbine*, Trondheim: Norwegian University of Science and Technology.
- DNV-GL, 2018. *DNV-GL-ST-0119: Floating Wind Turbine Structures*, Oslo: DNV-GL.

equinor, n.d. *How Hywind Works*. [Online]

Available at: <https://www.equinor.com/en/what-we-do/floating-wind/how-hywind-works.html>
[Accessed 12 April 2020].

Global Wind Energy Council, 2019. *Global Wind Report 2018*, Brussels: Global Wind Energy Council.

Haigh, S., 2020. *4D6 Lecture 5: Shear stiffness of dry and saturated soils*. Cambridge: s.n.

Hardin, B. & Drnevich, V., 1972. Shear Modulus and Damping in Soils: Design Equations and Curves. *Geotechnical Special Publication*, 98(118), pp. 667-692.

Houlsby, G. T., 2009. *Simplified Pile Capacity Design Calculations*. Oxford: University of Oxford.

IRENA, 2016. *Floating foundations: a game changer for offshore wind power*, Abu Dhabi: IRENA.

Jardine, R. J. & Standing, J. R., 2000. *Pile load testing performed for HSE cyclic loading study at Dunkirk, France - Volume 1*, London: Health and Safety Executive.

Jardine, R. J. & Standing, R. J., 2012. Field axial cyclic loading experiments on piles driven in sand. *Soils and Foundations*, 52(4), pp. 723-736.

Jardine, R. & Standing, J., 2000. *Pile load testing performed for HSE cyclic loading study at Dunkirk, France - Volume 2*, London: Health and Safety Executive.

Leblanc, C., Houlsby, G. T. & Byrne, B. W., 2010a. Response of stiff piles in sand to long-term cyclic lateral loading. *Geotechnique*, 60(2), pp. 79-90.

Liu, T., Aghakouchak, A., Taborda, D. M. G. & Jardine, R. J., 2017. *Advanced laboratory characterization of a fine marine sand from Dunkirk, France*. Seoul, Soil Mechanics and Geotechnical Engineering.

Mamo, B., Banoth, K. & Dey, A., 2015. *EFFECT OF STRAIN RATE ON SHEAR STRENGTH PARAMETER OF SAND*. Maharashtra, Indian Geotechnical Conference.

Matha, D., 2009. *Model Development and Loads Analysis of an Offshore Wind Turbine on a Tension Leg Platform, with a Comparison to Other Floating Turbine Concepts*, Boulder: National Renewable Energy Laboratory & University of Colorado.

Ng, C. & Ran, L., 2016. *Offshore Wind Farms: Technology, Design and Operation*. 1st ed. s.l.:Woodhead Publishing.

Oh, K.-Y. et al., 2018. A review on the foundation of offshore wind energy converters: current status and future perspectives. *Renewable and Sustainable Energy Reviews*, Volume 88, pp. 16-36.

Pegalajar-Jurado, A. et al., 2016. Experimental and numerical study of a 10MW TLP wind turbine in waves and wind. *Journal of Physics: conference Series*, 753(9), pp. 1-11.

Puech, A., 2013. *Advances in axial cyclic pile design: contribution of the SOLCYP project*. Paris, ISSMGE Technical Committee TC 209 .

Rovere, M., 2004. *Cyclic loading test machine for caisson suction foundations*. Oxford: s.n.

- Silva, M. et al., 2013. *Influence of cyclic axial loads on the behaviour of piles driven in sand*. Paris, ISSMGE Technical Committee TC 209.
- SOLCYP, 2012. *A Four-Year Joint Industry Project On the Behaviour of Piles Under Cyclic Loading*, London: Society of Underwater Technology.
- Suzuki, K. et al., 2011. Initial Design of Tension Leg Platform for Offshore Wind Farm. *Journal of Fluid Science and Technology*, 6(3), pp. 372-381.
- The Carbon Trust, 2015. *Floating Offshore Wind: Market and Technology Review*, London: The Carbon Trust.
- The Engineering Toolbox, n.d. *Young's Modulus - Tensile and Yield Strength for common Materials*. [Online]
Available at: https://www.engineeringtoolbox.com/young-modulus-d_417.html
[Accessed 10 April 2020].
- Thomassen, K., Ibsen, L. B. & Andersen, L. V., 2017. Laboratory Test Setup for Cyclic Axially Loaded Piles in Sand. *Electronic Journal of Geotechnical Engineering*, 22(3), pp. 1089-1106.
- Tsuha, C. et al., 2012. Behaviour of displacement piles in sand under cyclic axial loading. *Soils and Foundations*, 52(3), pp. 393-410.
- UK Government, 2019. *Climate Change Act 2008 (2050 Target Amendment) Order 2019*. London: UK Government.
- White, D. & Bolton, M., 2004. Displacement and strain paths during plane strain model pile installation in sand. *Geotechnique*, 54(6), pp. 375-397.
- Windpower Engineering and Development, 2018. *New U.S. patent granted for floating marine wind turbine*. [Online]
Available at: <https://www.windpowerengineering.com/new-u-s-patent-granted-for-floating-marine-wind-turbine/>
[Accessed 17 April 2020].
- Yang, J., 2006. Influence Zone for End Bearing of Piles in Sand. *Journal of Geotechnical and Geoenvironmental Engineering*, 132(9), pp. 1229-1237.
- Yue, M. et al., 2020. Effects of heave plate on dynamic response of floating wind turbine Spar platform under the coupling effect of wind and wave. *Ocean Engineering*, Volume 201.
- Zhao, Y., Yang, J. & He, Y., 2012. Preliminary Design of a Multi-Column TLP Foundation for a 5-MW Offshore Wind Turbine. *Energies*, 5(10), pp. 3874-3891.

8. Appendix A: Safety

In retrospect the risk assessment was successful at bringing to the author's attention the risks associated with the project, and the actions necessary to avoid them. This resulted in a safe working environment, in which none of the listed hazards – or any further unidentified hazards – came into fruition.

As well as this, the risk assessment did not go too far by unnecessarily restricting the progress of the project. For example, it allowed overnight tests. These were safe and invaluable to the project, but they would not have been allowed had their not been an appropriate assessment of risk.

The part of the risk assessment that the author believes to be most effective, was the identification of hazards in the Schofield Centre's working environment. Rather than focussing on the test rig and experimental procedure which were generally low risk, the risk assessment correctly identified hazards in the working environment, which generally posed a greater potential threat. These hazards were successfully mitigated by the risk assessment control measures, for example the use of dust masks when pouring sand and the avoidance of cordoned off workshop zones.

The Schofield Centre's cyclic test rig was less dangerous than had been identified. This was mainly because, when a pile was pulled from the ground, it happened slowly and remained in the soil. This meant that the Perspex screen that was going to be built around the rig was not necessary.

Overall, the risk assessment was successful, and the methodical, rational approach to identifying and analysing risk will be adopted in the author's future projects.

9. Appendix B: COVID-19 Disruption

Having spent Lent Term modifying the cyclic test rig and improving the pile design and installation, I was ready to start completing cyclic tests on Friday the 13th March, the last day of Lent Term. My intention was to complete some of the cyclic tests that week, stop for revision and exams, and then continue my final tests in Easter Term.

However, the Schofield Centre was forced to close at the end of that week due to COVID-19. I therefore had to collect all my data in what became a very fast paced, intense week. The tests I made in that week are the ones on which my report is based, and are detailed in the table below:

Coronavirus Affected Testing Timeline

Fri 13 th	Sat 14 th	Sun 15 th	Mon 16 th	Tues 17 th	Wed 18 th	Thur 19 th	Fri 20 th
Last day of term	Weekend – Schofield Centre Closed						Last day Schofield open
PO-S2-X PO-S2-1			PO-S2-2 PO-S2-3	CYC-E-1.5 CYC-N-1.5	CYC-N-3	CYC-N-2.25	CYC-E-2.25

I was sufficiently organised to collect all the data that I had originally planned to. However, not being able to return to the lab had some drawbacks, the main were:

- No possibility of running tests for more than 24hrs, and therefore having to stop CYC-N-2.25 and CYC-N-3 early before they reached shaft failure.
- No possibility of completing further cyclic tests beyond those initially planned (e.g. those described in the recommendations for further study).
- No possibility to re-test or account for loss of load-control during pull-out tests.
- No time to take high quality photos of the test rig.

Nevertheless, the data collected allowed the original objectives of the project to be met, and for that I am grateful.